7

Magnetic Adaptive Testing

Ivan Tomáš[1] and Gábor Vértesy[2]
[1]*Institute of Physics, Praha,*
[2]*Research Institute for Technical Physics and Materials Science, Budapest*
[1]*Czech Republic*
[2]*Hungary*

1. Introduction

Tests of impending material degradation of engineering systems due to their industrial service make an indispensable part of any modern technological processes. *Destructive tests* are extremely important. Their considerable advantage consists in their *straightforwardness*. In great majority of cases they *directly test the very property*, which is at stake. For instance, the limiting endurable stress before the material yields is directly measured by a mechanical loading test, or the number of bending cycles before the system breaks is directly counted to find the fatigue limits, and so on. Besides, the destructive inspections are regularly used in situations of any materialized failure, when knowledge of the *final condition* of the material at the moment of the breakdown helps to avoid any next malfunction of the same or similar systems under equivalent circumstances. However, the destructive tests cannot be used on the finished or half-finished parts in process of their industrial production, simply because those parts – after having been destructively tested – cannot be used for their primary purpose any more. The only possible application of destructive tests in industry is to examine destructively every n^{th} produced piece only, which is not sufficient for reliability of goods presently required.

Nondestructive tests, do not suffer by those problems. Causing no harm, they can be used at each produced object, and they can be periodically applied even on systems in service. Judging by the vivid interest in the presently observed improvement of traditional nondestructive tests and in development of some recently discovered ones, the nondestructive evaluation of material objects attracts currently attention perhaps even more than the destructive assessment does. Evaluation of nondestructive tests keeps the user informed about the *actual condition* of the system, and should ensure avoidance of any failure *before* it ever happens. There are numerous methods of nondestructive tests, based on optical, acoustic, electrical, magnetic and other properties of the materials, which can be *correlated* with the watched quality of the whole system. The necessity of the *unambiguous correlation* between the nondestructively measured physical property and the guarded property of the system at stake is an *unreservedly required* claim. It calls for the nondestructive tests to be examined and re-examined to their *one hundred percent reliability* before they can be really applied in crucial cases. Multi-parametric output of a nondestructive testing method is therefore an extremely valuable and welcomed property,

which enables to check and to cross-check validity of the necessary correlation and ensures reliability of single measurement with respect to the guarded physical quality of the tested system. The presently described method of Magnetic Adaptive Testing (MAT) is just one of the few *multi-parametric* nondestructive tests available.

Many industrial systems have construction parts, which are fabricated from the most common ferromagnetic construction materials, such as steel or cast iron. Nondestructive tests of their structural-mechanical quality can be very suitably based on magnetic measurements, because processes of magnetization of ferromagnetic materials provide detailed reflection of the material microstructure and its degradation.

The physical processes, which take place in the course of magnetization of ferromagnetic materials by an applied magnetic field, are well known. They are classified as reversible (mostly continuous changes of direction of the magnetization vector within magnetic domains) and irreversible (mostly discontinuous changes of volumes of magnetic domains, caused by jumps of domain walls from a position to a next one). These processes, the latter ones in particular, are closely correlated with structure of the sample, with its uniformity, texture, material defects, internal and external stresses and even with the sample shape. This can be disturbing, if we want to measure magnetic properties of the pure material. However, if we are interested just in the material structure, this correlation serves as a starting point of all magnetic techniques used for magnetic nondestructive tests of any ferromagnetic material. For detailed survey of such magnetic methods see e.g. papers (Jiles, 1988, 2001, Blitz, 1991, Devine, 1992) and many references to actual measurements quoted there.

Magnetic hysteresis methods belong to the most successful indirect ways of structural investigation of ferromagnetic construction materials. They are mostly based on detection of the material structural variations via variation of the traditional parameters of the *major,* saturation hysteresis loop, such as coercive field, H_C, remanent magnetic induction, B_R, maximum permeability, μ_{MAX}, and a few others. At first, these magnetic parameters are experimentally correlated with independently measured real structural / mechanical characteristics of the samples, and then from measurement of the former ones the latter can be determined. The point is that the magnetic parameters are measured *non-destructively and with less difficulty* than the real structural / mechanical characteristics, which in most cases can be learned destructively only. The few traditionally employed magnetic parameters are actually special points or slopes on the magnetic major hysteresis loop. These traditional parameters are very well suited for characterization of *magnetic properties* of ferromagnetic materials, but they were *never optimized* for magnetic reflection of modified *structural properties* of the measured samples. Besides, they are by no means the only available magnetic indicators of various nonmagnetic modifications of ferromagnetic materials. Correlation between alternative magnetic parameters and concrete structural changes of the studied material, can possibly be even *better adapted* to each specific task.

Structural aspects of ferromagnetic samples cover material non-uniformities such as local mechanical stresses, clusters of dislocations, grains, cavities, inclusions and many others. Their presence, distribution and magnitude control details of the magnetization processes, and there is no reason to expect that each type of structural defect affects all regions of each magnetization process with the same intensity. Measurement of a suitably chosen magnetic

variable, e.g. magnetic induction, B, or differential permeability, μ, of differently degraded samples of the same material, while changing the applied field in a systematic way, confirms the fact. Analysis of a large *family of minor hysteresis loops* is a good example of such a systematic investigation of magnetization processes. Besides, as known from the Preisach model of hysteresis (Bertotti, 1998), such volume of data is able to make a complete magnetic picture of the sample.

A novel method, Magnetic Adaptive Testing (MAT), for magnetic nondestructive inspection of ferromagnetic construction materials (Tomáš, 2004) is introduced in this chapter. The method is based on systematic measurement of minor magnetic hysteresis loops. The essential difference between material testing by the traditional hysteresis- and by the MAT-approach is shown in Fig. 1 schematically. The left hand part of the figure represents the traditional measurement of the *single major* (saturation) hysteresis loop. The major loop is measured for each of the degraded samples and the material degradation can be described through variation of values of any *of the few major loop parameters*, e.g. H_C, B_R, ... as functions of an independent degradation variable, ε, (e.g. as functions of mechanical tension). The right hand part of the figure depicts schematically volume of the measured data for MAT. The large family of minor hysteresis loops is measured for each of the degraded samples and the material degradation can be then described through variation of values *of any of the point (and/or slope) on any of the minor loops*, i.e. $B(F_i, A_j)$ (and/or $\mu(F_i, A_j)$), as functions of an independent degradation variable, ε, (e.g. as functions of mechanical tension).

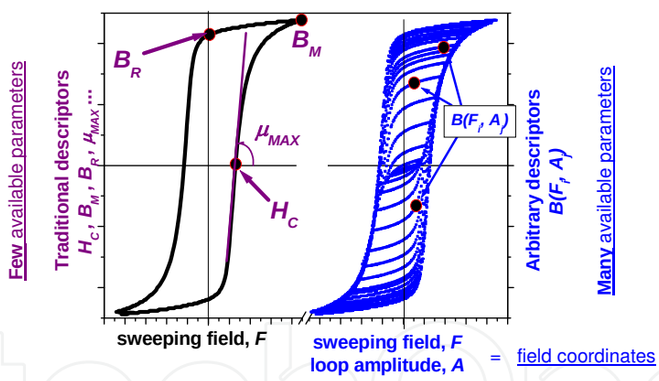

Fig. 1. Schematic comparison of the traditional magnetic hysteresis testing (left) and Magnetic Adaptive Testing (right). The traditional testing uses only a few parameters of the major loop for description of the material. Magnetic Adaptive Testing has the choice to pick up the best from many available parameters indexed by the field coordinates.

The method of Magnetic Adaptive Testing utilizes systematic measurement of large families of minor hysteresis loops, from minimum amplitudes up to possibly the maximum (major) ones on degraded ferromagnetic samples/objects. From the large volume of the recorded data, those are applied for *evaluation* of the degradation, which reflect the material degradation in the most sensitive or otherwise the most convenient way. Such – *best adapted for the investigated case* – data are used as the MAT-parameter(s) and its / their dependence on an independent variable accompanying the inspected degradation is referred to as the

MAT degradation function(s). The following text is dedicated to description of basic principles of MAT, to specific advantages and disadvantages of the method and to a number of cases when MAT was successfully applied.

2. Description of the method

The basic features and processes of use of the method of Magnetic Adaptive Testing are probably most instructive and easy to understand, if they are demonstrated on a typical concrete example of MAT application. Therefore, throughout Section 2, properties are described of samples manufactured from low carbon steel, which was degraded (plastically deformed) by previous application of 7 different magnitudes of mechanical tension. The seven steel samples are ring-shaped with the magnetizing and the pick-up coils wound on each of them. All the figures presented in Section 2 refer to this example.

The magnetic induction method appears to be the easiest way of the systematic measurement for MAT. A Permeameter described in Fig. 2 makes a practical example of the possible experimental arrangement. The driving coil wound on the magnetically closed sample gets a triangular waveform current with stepwise increasing amplitudes and with a fixed slope magnitude in all the triangles (see Fig. 2, right). This produces a triangular variation of the magnetizing field with time, t, and a voltage signal, U, is induced in the pick-up coil for each k^{th} sample:

$$U(\mathrm{d}F/\mathrm{d}t, F, A_j, \varepsilon_k) = K^*\partial B(\mathrm{d}F/\mathrm{d}t, F, A_j, \varepsilon_k)/\partial t = K^*\mu(\mathrm{d}F/\mathrm{d}t, F, A_j, \varepsilon_k)^*\,\mathrm{d}F/\mathrm{d}t, \qquad (1)$$

where K is a constant determined by geometry of the sample and by the experimental arrangement. As long as $F=F(t)$ sweeps linearly with time – i.e. $|\mathrm{d}F/\mathrm{d}t|$ is (the same) constant for measurement at each of the samples, Eq.(1) states, that the measured signal is simply proportional to the differential permeability, μ, of the measured magnetic circuit, as it varies with the applied field, F, within each minor loop amplitude, A_j, for each k^{th} measured sample. If correct results without influence of any previous remanence should be obtained, it is evident that each sample has to be thoroughly demagnetized before it is measured.

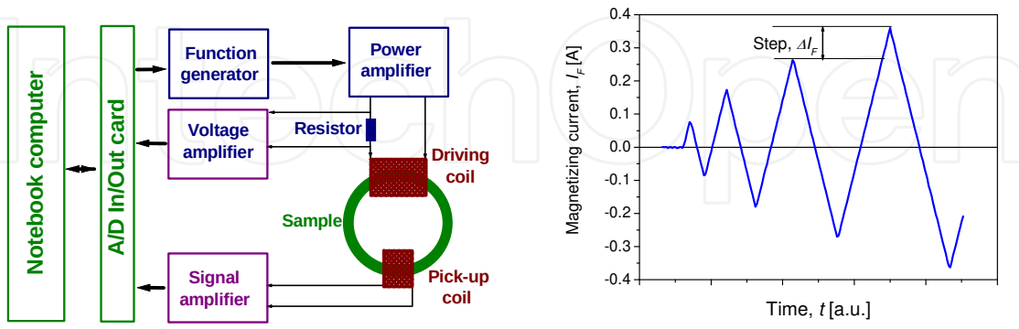

Fig. 2. Left: Block-scheme of the Permeameter. The driving coil produces triangular variations of the applied magnetic field. The signal coil picks-up the induced voltage proportional to differential permeability of the sample. This scheme shows arrangement when a magnetically closed sample is measured and both the coils are wound directly on the sample. Right: Triangular variation of the magnetizing current with time.

The Permeameter works under control of a notebook PC, which sends the steering information to the function generator and collects the measured data. An input/output data acquisition card accomplishes the measurement. The computer registers actually two data files for each measured family of the minor μ-shaped loops. The first one contains detailed information about all the pre-selected parameters of the demagnetization and of the measurement. The other file holds the course of the voltage signal, U, induced in the pick-up coil as a function of time, t, and of the magnetizing current, I_F, and/or field, F. A typical example of one family of the μ-shaped loops (the reference, unstrained sample with ε_0=0%) is shown in Fig. 3a, and Fig. 3b presents the seven families of all the seven ring samples of the steel degraded by the previously applied mechanical tension to the strain values ε_k = 0%, 1.7%, 3.5%, 5.8%, 7.8%, 9.8%, 17.9%, respectively. Evidently it is a lot of data and our task is to compare them and to find the most suitable ones for description of the investigated material degradation.

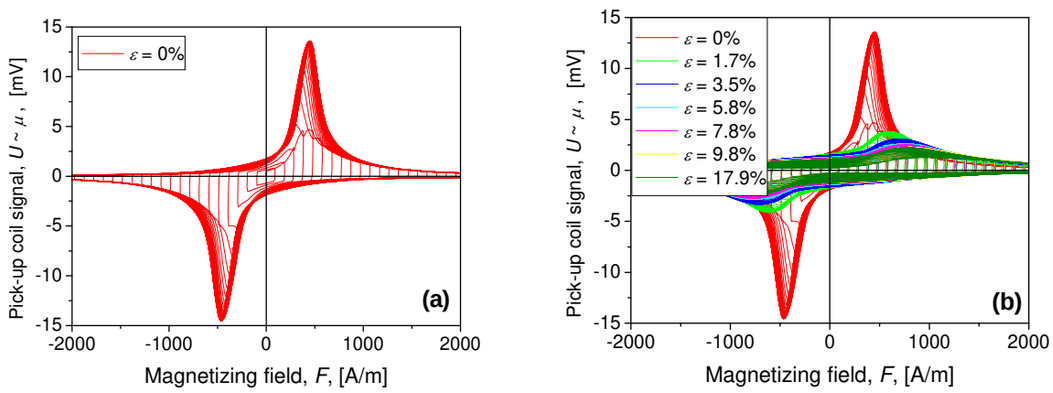

Fig. 3. Examples of families of the μ-shaped loops vs. magnetizing field, F. (a) Measured on the unstrained – ε_0=0% – low carbon steel sample. The positive and negative parts of the signal correspond to the increasing and decreasing parts of the triangular waveform of the current (field), respectively. (b) Measured on all the seven ring samples, manufactured from low carbon steel, which was degraded by mechanical tension down to strain values ε_k = 0%, 1.7%, 3.5%, 5.8%, 7.8%, 9.8%, 17.9%. The curves are plotted in dependence on the magnetizing field, F, within the limits ± 2000 A/m.

Instead of keeping the signal and the magnetizing field in shapes of continuous time-dependent functions, it is practical to interpolate the family of data for each ε_k-sample into a discrete square (i, j)-matrix, $U(F_i, A_j, \varepsilon_k)$, with a suitably chosen step, $\Delta A = \Delta F$. (Because $\mathrm{d}F/\mathrm{d}t$ is a constant, identical for all measurements within one experiment, it is not necessary to write it explicitly as a variable of U.) MAT is a relative method (practically all the nondestructive methods are relative), and the most suitable information about degradation of the investigated material can be contained in variation of *any* element, of such matrices as a function of ε, relative with respect to the corresponding element of the reference matrix, $U(F_i,A_j,\varepsilon_0)$. Therefore all $U(F_i, A_j, \varepsilon_k)$ elements will be divided by the corresponding elements $U(F_i,A_j,\varepsilon_0)$ of the reference sample matrix and *normalized* elements of matrices of relative differential permeability $\mu(F_i,A_j,\varepsilon_k) = U(F_i, A_j, \varepsilon_k)/U(F_i, A_j, \varepsilon_0)$, and their proper sequences

$$\mu(F_i,A_j,\varepsilon) = U(F_i, A_j, \varepsilon)/U(F_i, A_j, \varepsilon_0) \quad (2)$$

as *normalized* μ*-degradation functions* of the inspected material will be obtained. Throughout the text of this chapter, all the degradation functions are considered as *normalized* with respect to the corresponding values of the reference sample.

Beside the μ-matrices and the corresponding μ*-degradation functions*, also matrices of the integrated, $B=\int \mu dF$, or the differentiated, $\mu'_F=\mathrm{d}\mu/\mathrm{d}F$, and/or $\mu'_A=\mathrm{d}\mu/\mathrm{d}A$ values can be computed and used for definition of the *B-degradation functions*, $B(F_i,A_j,\varepsilon)$, of the μ'_F*-degradation functions*, $\mu'_F(F_i,A_j,\varepsilon)$, and/or of the μ'_A*-degradation functions*, $\mu'_A(F_i,A_j,\varepsilon)$. In fact the *B*-, μ'_F-, and μ'_A-degradation functions do not contain more or other information than the μ-degradation functions, but their use is sometimes more helpful and they are occasionally able to show certain material features with higher sensitivity or in different relations. This will be shown later in the application examples. (Note: As the μ'_A–degradation functions are actually not used in any of the examples here, μ'_F is simply denoted as μ' thoughout this chapter.) In some cases it turns out, that degradation functions of *reciprocal* values, such as $1/\mu$-degradation functions and the similar others, are more convenient than the direct ones. Application of the reciprocal degradation functions proves effective especially in situations when – with the increasing parameter ε – the direct degradation functions approach kind of a "saturation".

An example of the μ-degradation functions and $1/\mu$-degradation functions of the low carbon steel degraded by the mechanical tension is shown in Fig. 4.

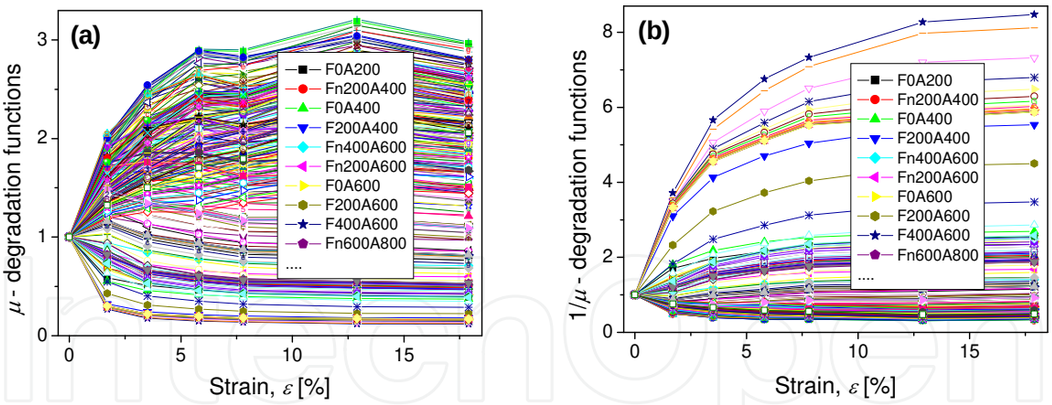

Fig. 4. The μ-degradation functions (a) and $1/\mu$-degradation functions (b) of the low carbon steel degraded by the mechanical tension. The functions were calculated for the step $\Delta A = \Delta F$ = 200A/m and they are plotted up to the maximum amplitude A_j = 3600 A/m.

Number of the degradation functions obtained from the MAT measurement depends on magnitude of the maximum minor loop amplitude, A_j, up to which the measurement is done, and on choice of the step value $\Delta A = \Delta F$ which is used for computation of the interpolated data matrices. The maximum amplitude A_j = 3600 A/m and the step $\Delta A = \Delta F$ = 200 A/m were applied in the presented example of investigation of the degraded steel. Under these conditions there are altogether 289 exploitable μ-degradation functions (all the

unreliable "boundary" (F_i=±A_j) degradation functions were excluded from the total number of $_{n=0}\Sigma^{n=17}(2n+1)=324$) and the same number of $1/\mu$-degradation functions, as they are plotted in Fig. 4.

Once the degradation functions are computed, the next task is to find the *optimum* degradation function(s) for the most sensitive and enough robust description of the investigated material degradation. A 3D-plot of sensitivity of the degradation functions can substantially help to choose the optimum one(s). The μ- and $1/\mu$-sensitivity maps corresponding to the degradation functions of Fig. 4 are plotted in Fig. 5. Slope of the linear regression of each degradation function is here defined as the function sensitivity. Thus the *sensitivity map* is a 3D-graph of these slope values plotted against the degradation functions field coordinates (F_i, A_j). As it follows from the presented sensitivity maps, the most sensitive μ-degradation functions are those with field coordinates around (F_i=-1400 A/m, A_j=3600 A/m), and/or (F_i=2200 A/m, A_j=3600 A/m), whereas the most sensitive $1/\mu$-degradation functions evidently have the F-coordinate equal to F_i = 400 A/m and the optimum amplitudes start from A_j = 600 A/m (the most sensitive $1/\mu$-degradation function) and the sensitivity decreases (but keeps rather high anyway) for larger minor loop amplitudes. The most sensitive μ- and $1/\mu$-degradation functions are plotted in Fig. 6.

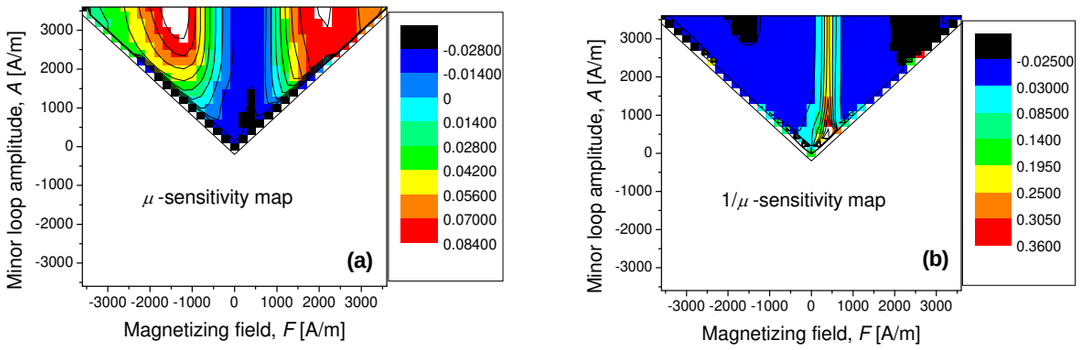

Fig. 5. The μ-sensitivity map (a) and $1/\mu$-sensitivity map (b) of the low carbon steel degraded by the mechanical tension. The maps were calculated for the step ΔA = ΔF = 200 A/m and they are plotted up to the maximum amplitude A_j = 3600 A/m.

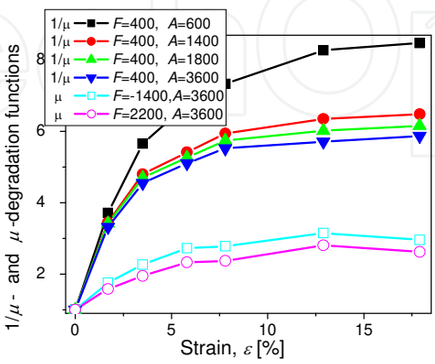

Fig. 6. The most sensitive degradation functions for plastic deformation of a steel for the step ΔA = ΔF = 200 A/m. The top sensitive is the $1/\mu$-degradation function with field parameters F_i = 400 A/m, A_j = 600 A/m. The most sensitive μ-degradation functions are more flat.

3. Methodological hints

During measurement of the induced signal in the example presented in previous Section, samples shaped like thin rings were used, and the magnetizing and the pick-up coils were wound directly on them. Relatively *small field* was able to magnetize the material substantially, as there was *no demagnetization* effect, and *homogeneous magnetization* of the sample material was rightfully assumed. Signal measured on such *magnetically closed* samples is proportional to differential permeability of the samples *material*, and magnetizing field, *F*, *inside* the samples can be easily calculated as

$$F = N\, I_F/L \qquad [\mathrm{A/m}, 1, \mathrm{A}, \mathrm{m}], \tag{3}$$

where N is number of turns of the magnetizing coil, I_F is the magnetizing current and L is circumferential length of the magnetic circuit (e.g. of the sample ring).

If the measured samples are *magnetically open*, the situation is more complicated. "Long and narrow" specimens can be also successfully magnetized by coils placed *around* their body, as the demagnetization of such shapes is still acceptable for the MAT measurement. However, demagnetization field comes here into picture and the total inside field cannot be calculated as easily as suggested by Eq.(3). And what to do with short stout or large flat shapes? The magnetic circuit of such samples can be artificially closed, and the samples can be magnetized and measured with the aid of a magnetically soft yoke. The yoke can be either *passive* with the coils wound around body of the sample, or the yoke can be *active* (we speak then about an active *inspection head*) with the magnetizing coil wound around the bow of the yoke and the pick-up coil around one or both legs of the yoke.

Problems may appear in cases of rough or uneven surfaces of samples, where quality of magnetic contact between the sample and the yoke fluctuates from sample to sample. This introduces fluctuation of quality of the magnetic circuit and therefore also of the pick-up signal, which can be mistaken for variation of the samples material. The most rigorous solution of such situation is then simultaneous measurement of the tangential field on the sample surface (Stupakov, 2006, Stupakov et al., 2006, Perevertov, 2009), which substantially complicates the experiment, however. Another approach, which is able to solve the problem satisfactorily in majority of situations is to insert a non-magnetic spacer between the sample / yoke touching surfaces. The spacer makes the fluctuation relatively smaller and allows successful MAT measurement even on rough surfaces of magnetically open samples, see (Tomáš et al., 2012) and Section 3.5. However, fortunately, in great majority of investigated samples the different pieces of sample series have more-or-less similar quality of surface, which ensures reliable and repeatable measurements, even if the surface is rough, considering that MAT is a relative measurement, and degradation functions are normalized with the corresponding value of the reference sample.

In MAT measurements with open samples and attached yokes we deal with non-uniform magnetization. As a consequence, the magnetizing field inside the sample cannot be easily calculated like (3), we cannot use the magnetizing *field* coordinates (F_i, A_j), but we use the magnetizing *current* coordinates (I_{Fi}, I_{Aj}) instead. Besides, with the non-uniform magnetic circuits we cannot speak about the signal U to be proportional to the differential permeability of the *material*, but evidently we deal with an *effective* differential permeability

of the existing *circuit* instead. As MAT is a *relative* method, the current coordinates are also well applicable for identification of the mutually corresponding magnetic states of the samples to be related and compared.

Measurements on closed samples and on open ones, either in a solenoid or helped by attached yokes, evidently yield quantitatively different data. If measured on identical materials, are they comparable? Do they show similar trends? Next two Sections of this part give answers to such questions and describe MAT measurements performed on equivalent series of closed and open samples (Section 3.1) and on the same series measured in a solenoid and with the aid of yokes (Section 3.2). The remaining Sections of this part present several other points of the methodological discussion, namely the potential of multi-parametric character of MAT (Section 3.3), the influence on MAT sensitivity of speed of magnetization (Section 3.4) and of nonmagnetic spacers (Section 3.5), and eventually the influence of sample material temperature on the MAT results (Section 3.6). The last Section of this part, Section 3.7, refers to several traditional hysteresis and Barkhausen measurements of degraded samples and compares their results with those obtained by MAT.

3.1 Magnetically closed and open samples

Structural degradation of samples manufactured from compressed steel are here studied by MAT and their optimal $1/\mu$-degradation functions are compared with their rolling reduction, and with their independently measured Vickers hardness (HV). The material is low-carbon steel with 0.16 wt.% of C, 0.20 wt.% of Si, 0.44 wt.% of Mn, with the rest of Fe, and the samples were produced from steel plates cold rolled down to 0, 5, 10, 20 and 40% reduction. Three sample geometries are used, namely picture-frames, rectangular plates and rectangular bars. Dimensions and shapes of the samples are shown in Fig. 7.

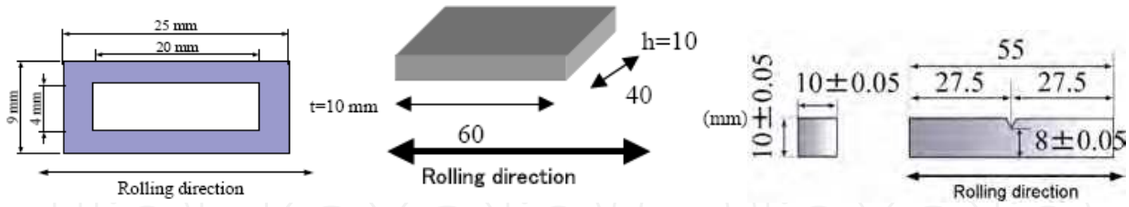

Fig. 7. Dimensions and shapes of the frames, of the plates and of the bar-samples.

MAT measurements were performed on all the samples. The frame samples were equipped with identical magnetizing and pick-up coils each. All plate- and bar-samples were measured by the same inspection head, directly attached (no non-magnetic spacers were used for the polished surfaces) on a surface of each sample. The optimum $1/\mu$-degradation functions were taken for each series of the samples. Representative sets of such optimal $1/\mu$-degradation functions vs. rolling reduction and vs. the Vickers hardness are plotted in Fig. 8 for the frame-, for the plate- and for the bar-shaped samples. In each measurement series, all the degradation functions are normalized by data of the virgin (not rolled) sample of the relevant shape. As seen from Fig. 8, consecutive series of the optimal MAT degradation functions well reflect the material modifications, regardless of the actual sample shapes. The results on series of differently shaped samples agree with

each other *qualitatively*, and the frame-shaped magnetically closed samples show the highest sensitivity, as expected. For making the measurements also *quantitatively* comparable and repeatable, it is necessary to perform the tests always under the same experimental conditions (speed of magnetization, steps of increasing current, etc.), to use the same measuring head (and/or the same coils), and evidently also the same shape of samples (see also Vértesy et al., 2008a).

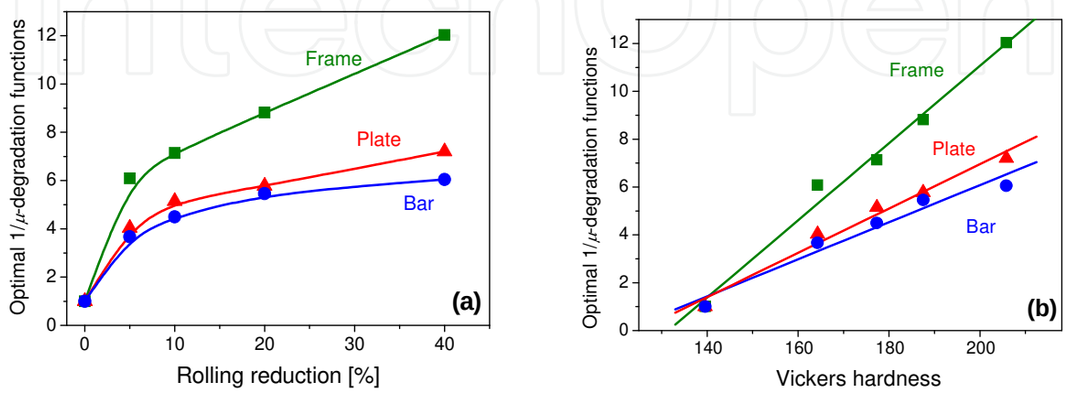

Fig. 8. Optimal *1/μ*-degradation functions for the three series of differently shaped samples. (a) Dependence on the rolling reduction. (b) Dependence on Vickers hardness.

3.2 Open samples between yokes and in a long solenoid

Low carbon commercial steel CSN 12050 was plastically elongated in an Instron loading machine up to final strain values 0, 0.1, 0.2, 0.9, 1.5, 2.3, 3.1, 4.0, 7.0 and 10.0%. A single series of identically shaped long flat samples (115x10x3 mm^3) was manufactured from the degraded steel pieces and it is here studied by MAT in two different ways, both applicable for these magnetically open samples. In one measurement series the samples were magnetized by a short coil, placed around middle of each sample and the magnetic circuit was artificially closed from both sides of the sample by two symmetrically positioned passive yokes (no non-magnetic spacers). The arrangement is shown in Fig. 9a, while Fig. 10a shows pick-up coil signals of the investigated samples. In the other measurement series the same samples were magnetized as open, in a long solenoid. This solenoid, with one of the samples inside, is shown in Fig. 9b. Fig. 10b demonstrates the pick-up coil signals originating from this experimental arrangement.

Dramatic quantitative differences can be observed between signals of Figs. 10a and b, even though the double-peak character of the signal is qualitatively preserved in both. And, in spite of difference between the directly measured signals, character of the MAT degradation functions vs. plastic strain is again qualitatively the same. It is shown in Fig. 11, where the optimal 1/μ-degradation functions of the discussed two cases are compared. Evidently, sensitivity of measurements is significantly higher if the samples are at least artificially closed by the yokes, but even in the worse case of the open long thin samples in a solenoid the material degradation is well measurable.

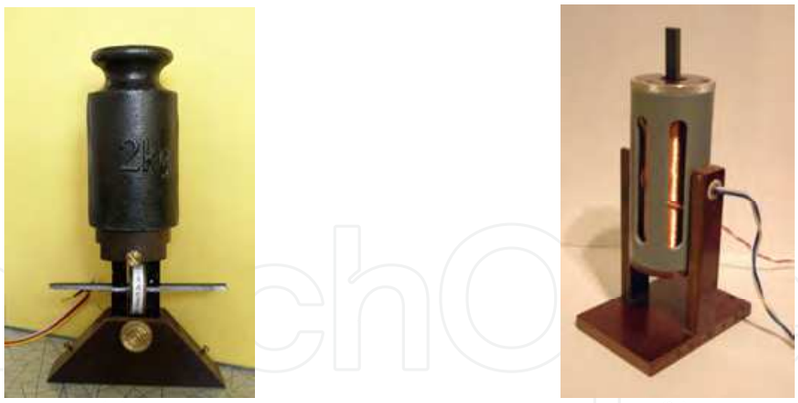

(a) (b)

Fig. 9. The arrangements, used for the measurements. (a): The samples are magnetized by the short coil placed around middle of each sample and a pair of soft passive yokes closes the magnetic circuit from bottom and top. (The 2 kg weight is used only for pressing the yokes better on the sample surfaces.) (b): The samples are magnetized inside the long solenoid.

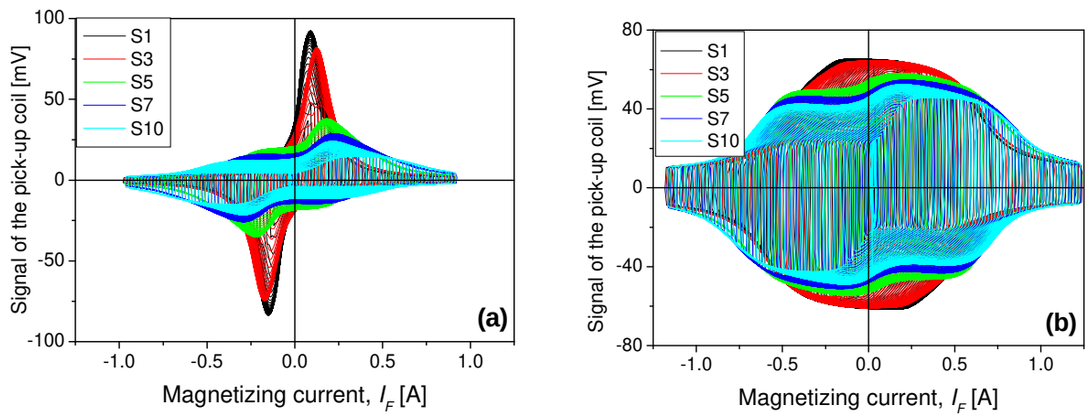

Fig. 10. Several pick-up coil signals of the investigated samples. (S1 is the reference, not deformed sample, S10 is the sample with 10 % strain). (a): Samples with artificially closed magnetic circuit by a pair of passive yokes. (b): Open samples in the solenoid. Remark: Scales in the (a) and (b) figures are not mutually comparable as neither the magnetizing solenoids nor the pick-up coils are the same in the two experimental arrangements.

3.3 Full use of the multi-parametrical character of MAT

Magnetic Adaptive Testing offers a great number of degradation functions. Usually *those* degradation functions are used as calibration curves for assessment of unknown samples, which are *monotonous and most sensitive* to the investigated material degradation. However, in some cases, magnetic reflection of the degraded material yields *only non-monotonous* degradation functions, see e.g. study of low cycle fatigue in (Devine et al., 1992, Tomáš et al., 2010). A single non-monotonous degradation function does not allow to decide whether a measured unknown sample belongs to the ascending or to the descending part of it. It will

be shown in this Section, that the multi-parametric behavior of MAT can solve this question and that a suitable combination of two or more non-monotonous degradation functions obtained from a *single* MAT measurement makes such a decision possible, see also (Vértesy & Tomáš, 2012a).

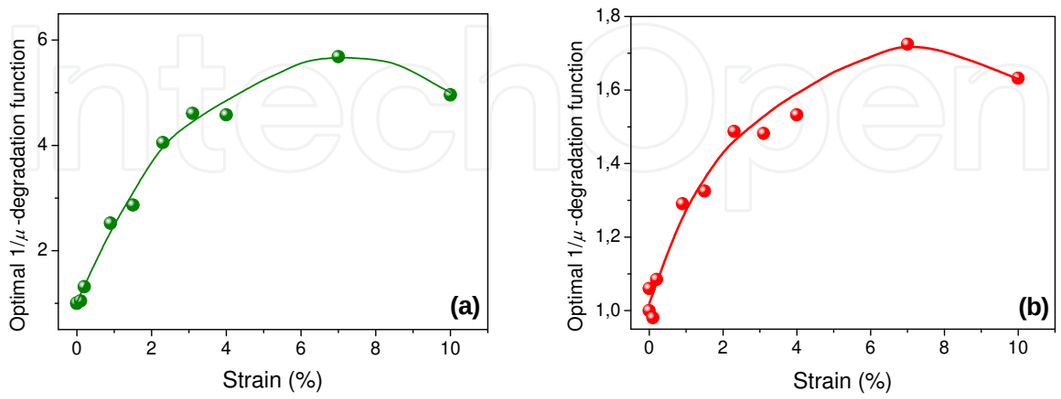

Fig. 11. MAT degradation functions vs. the plastic strain obtained on the tensile stressed steel samples. (a): Samples were artificially closed by a double yoke. (b): Open samples in the solenoid.

As an illustration of such a solution again the series of long flat samples (115x10x3 mm^3) is presented, which were manufactured from the commercial steel CSN 12050, plastically deformed by tensile stress up to the ten strain values 0, 0.1, 0.2, 0.9, 1.5, 2.3, 3.1, 4.0, 7.0 and 10.0%. The same samples were used in Section 3.2 already for demonstration of equivalency between results of two different ways of measurement. Data from the arrangement with two passive yokes (see Fig. 9a) are described here.

The non-monotonous character of the *1/μ*-degradation functions is shown in Fig. 11, and the same is true about the *1/μ'*-degradation functions, which are presented in Fig. 12. The most sensitive *1/μ'*-degradation functions come from the area of coordinates around I_F=40 mA, I_A=150 mA values (see the red area in the *1/μ'*-sensitivity map plotted in Fig. 13), but as shown in Fig. 12a, they are non-monotonous at the range of large strains. If *1/μ'*-degradation functions from other areas of the sensitivity map are plotted, all of them show the non-monotonous shape as well. However, not all of them have the peaks in the same range of strains as the most sensitive ones do. An example of such a *1/μ'*-degradation function is plotted in Fig. 12b. The function in Fig. 12b comes from the area around I_F =400 mA, I_A =600 mA (see the yellow area at the right-hand-side in the *1/μ'*-sensitivity map in Fig. 13.), it is substantially less sensitive than the optimal *1/μ'*-degradation function of Fig. 12a, but it is nicely monotonous at large strains (and non-monotonous at low strains, where the sensitive function does not have any problem). Evidently, the sensitive *1/μ'*-degradation function of Fig. 12a can be used as the *main* calibration function, but if an unknown sample falls into its non-monotonous part, the auxiliary *1/μ'* -degradation function of Fig. 12b answers the question about whether the unknown sample belongs to the ascending or to the descending part of the Fig. 12a-curve.

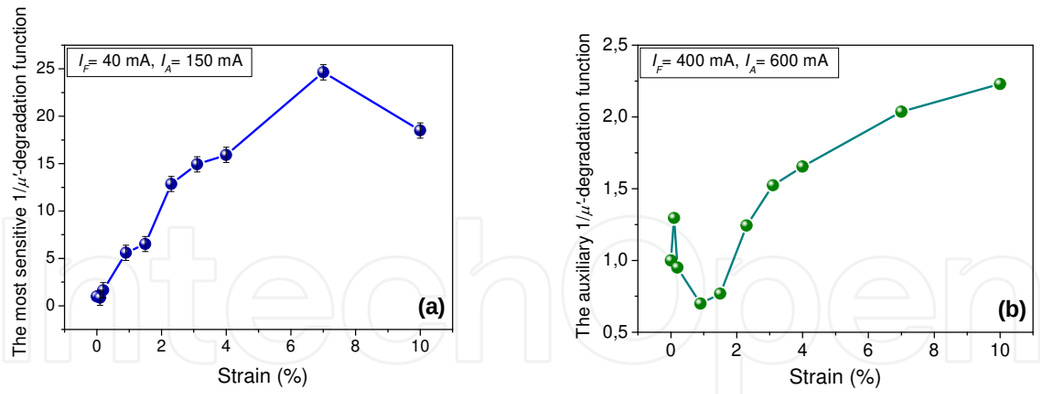

Fig. 12. (a): The optimum 1/μ′-degradation function from the (I_F=40 mA, I_A=150 mA) area. (b): The auxiliary 1/μ′-degradation function from the (I_F =400 mA, I_A =600 mA) area.

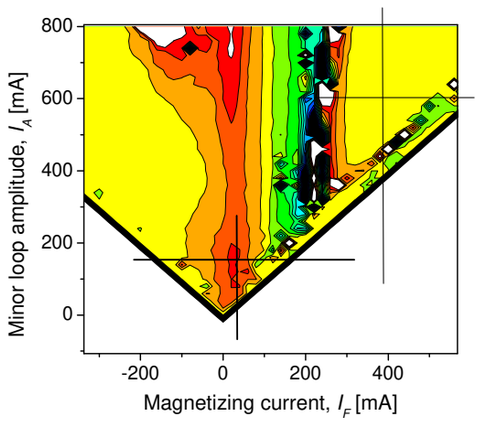

Fig. 13. The 1/μ′-sensitivity map of the steel degraded by tensile stress. Crossing lines indicate the areas from where degradation functions of Fig. 12 were taken.

3.4 Speed of magnetization

The most frequent way of MAT measurement proceeds by the electromagnetic induction method in a Permeameter similar to the scheme in Fig. 2 under the condition $|dF/dt|$=const. This condition guarantees that the magnetization processes in the samples continue always at the constant speed, which is desirable. As according to Eq.(1) the measured signal is directly proportional to dF/dt, this field-slope is set *high enough* with the intention of getting a sufficient signal-to-noise ratio. At the same time, however, it is advisable to set it *low enough* in order to minimize eddy currents and other dynamic effects, which can adversely influence shape of the signal and of the degradation functions via their implicit dependence on the value of dF/dt. In this Section influence of the rate of change of the magnetization processes on sensitivity of degradation functions in Magnetic Adaptive Testing will be investigated, see also (Tomáš et al., 2009).

The samples employed for this investigation were the same series of circular rings of low carbon steel plastically deformed by uniaxial tension, which was introduced as an illustrative example in Section 2. Arrangement of the experiment coincided with Fig. 2, so

that the varying magnetization of each sample was achieved by application of a time-dependent magnetic field, $F(t)$, due to triangular waveform current, $I_F(t)$, in the magnetizing coil, with step-wise increasing field-amplitudes, A_j, corresponding to the step-wise increasing current-amplitudes, I_{Aj}. The rate of change in all the triangles was constant (but for its sign), namely dI_F/dt=const. for the current-slope and/or dF/dt=const. for the magnetizing field-slope, in each measured family of the minor loops and in any measurements mutually compared. Three measurements of the same series of samples were carried out. The applied current-slopes and the corresponding field-slopes in the three measurements were dI_F/dt = 0.5 A/s, 4 A/s, 32 A/s, and dF/dt = 0.8 kA/m/s, 6.4 kA/m/s, 51.2 kA/m/s, respectively.

The sensitivity maps of the μ- and of the $1/\mu$-degradation functions computed for the measurement with the lowest field-slope dF/dt = 0.8 kA/m/s were plotted in Fig. 5 for the field-coordinates $-A_j \le F_i \le +A_j$, $0 < A_j \le 3.6$ kA/m, with the step $\Delta A = \Delta F = 0.2$ kA/m. The μ- and of the $1/\mu$-sensitivity maps for dF/dt = 6.4 kA/m/s, and 51.2 kA/m/s were qualitatively similar to those in Fig. 5. Three interesting regions of the field-coordinates (F_i, A_j) can be seen in each of the sensitivity maps, with slight shifts of the extreme regions due to different field-slopes. The white regions in Fig. 5a indicate the most sensitive *increasing* μ-degradation functions, the black areas indicate the most sensitive *decreasing* μ-degradation functions. For the $1/\mu$-degradation functions (see Fig. 5b) it naturally is just reversed. The most sensitive degradation functions for the field-slope dF/dt = 0.8 kA/m/s are plotted in Section 2. in Fig. 6. The same degradation functions, together with their counterparts for higher values of the field slope, namely for dF/dt = 6.4 kA/m/s, and 51.2 kA/m/s are drawn in Fig. 14 in the present Section.

As the curves in Fig. 14 show, there is very little influence of the varied magnetizing field-slope from 0.8 till 51.2 kA/m/s (i.e. 64 times larger speed of magnetization) on sensitivity of the best μ-degradation functions within their regions of monotonous *increase* (i.e. in the two "white" areas of the sensitivity map of Fig. 5a). However, the best degradation functions from the "white" region of Fig. 5b, (i.e. those with a monotonous *increase* of the $1/\mu$-degradation functions) are influenced substantially as it is seen on Fig. 14c. As the degradation functions are created by the signals ratio shown in Eq. (2), explanation of this behavior can be found through a closer look at the recorded induced voltage signals both for the degraded samples, ε_k, and for the normalizing reference sample, ε_0, as was discussed in details in (Tomáš et al., 2009).

There is no universal advice as for what magnetizing field-slope to chose and what region of degradation functions to use for the most successful MAT nondestructive tests in individual cases. As the name of the method suggests, it is recommended to *adapt* optimally the choice both of the degradation functions field-coordinates region and the magnetizing field-slope as to obtain the satisfactory signal-to-noise ratio and the best degradation function sensitivity at the same time. The concrete adaptation is completely governed by properties of the investigated material degradation and by the level of noise and the available rate of change of the magnetizing field of the used measuring technique.

However, generally speaking it can be stated, that as long as the MAT degradation functions are picked-up from localities of the field coordinates where the local differential permeability is *high* (frequently close to the maximum permeability at the used minor loop),

then the (usually "reciprocal") degradation functions possess *very high sensitivity*, but level of their sensitivity is *strongly field-slope-dependent*. On the other hand, if the MAT degradation functions are chosen from localities of the field coordinates where the material is closer to saturation and the local differential permeability is *low*, sensitivity of such degradation functions is *not extremely high*, but it is *little dependent on the applied magnetizing field-slope*.

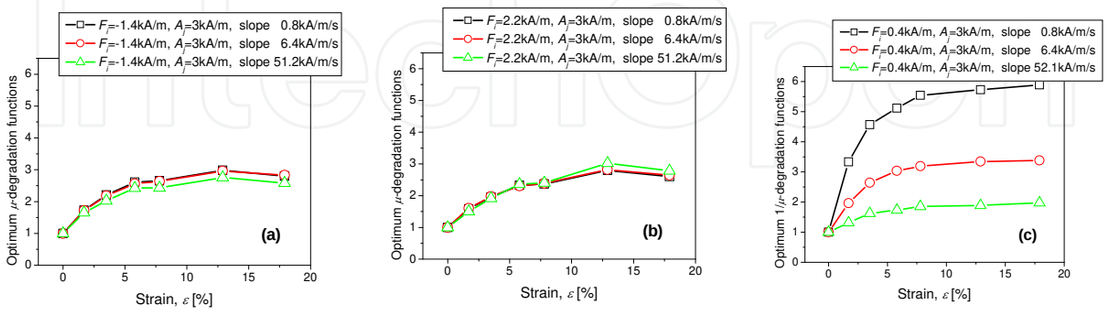

Fig. 14. The steepest degradation functions measured at the three magnetizing field-slopes dF/dt = 0.8 kA/m/s (□), 6.4 kA/m/s (O), and 51.2 kA/m/s (Δ), at the three important coordinate regions of the sensitivity maps. For easy comparison all the degradation functions are determined at the minor loop with amplitude A_j = 3kA/m: $\mu(F_i,A_j,\varepsilon)$ at F_i = -1.4 kA/m (a), $\mu(F_i,A_j,\varepsilon)$ at F_i = +2.2 kA/m (b), and $1/\mu(F_i,A_j,\varepsilon)$ at F_i = +0.4 kA/m (c).

3.5 Non-magnetic spacers

Magnetic measurement of flat samples, which cannot be magnetized (and/or closed magnetically) in any better way than by an attached magnetizing/sensing soft yoke, set into direct contact with the sample surface, suffers often by fluctuation of quality of the magnetic sample/yoke contact. This is a well-known problem, with unpolished surfaces in particular, which can be improved by using as large yoke as possible and/or by application of a spacer between the yoke and the sample. However, size of the sample frequently does not allow a very large yoke to be used and even a thin nonmagnetic spacer decreases and distorts the measured signal substantially, so that measurement of basic *magnetic parameters* of the sample material in this way is very difficult, if not impossible.

However, spacers are quite applicable for magnetic "structuroscopy", i.e. for magnetic measurement of relative structural changes of ferromagnetic construction materials, especially if the measurement is carried out by a method analyzing the measured signal like it is done e.g. in Magnetic Adaptive Testing. The following measurement explains and illustrates use of spacers, see also (Tomáš et al., 2012).

Samples of gradually increasing brittleness were prepared from ferromagnetic steel 15Ch2MFA in the shape of rectangular prisms 10 x 10 x 30 mm^3. Material for the samples was embrittled in the same way as described in Section 4.3.2. Three samples of each grade of brittleness (of the same tempering temperature T_T of their preparation, see Section 4.3.2) were used for the reported measurement. Quality of surfaces of the samples corresponded to their ordinary machining (milling) and grooves from the milling or even scratches were visible on some of them. No polishing of the surfaces was implemented, some surfaces were evidently worse than others.

The measurement was done inductively on the magnetically open samples using a pair of passive yokes. Magnetization of the samples was carried out by a short driving coil, which was each of the samples before the measurement inserted into. The induced voltage signal was recorded from a pick-up coil, placed co-axially with the driving one. In order to be able to magnetize the short thick samples by the small driving coil appreciably, two soft yokes of laminated Si-Fe sheets (cross sections of the legs 10x20 mm^2, maximum height in the bow 30 mm) were used to short-cut the magnetic flux during magnetization of the samples. The yokes were attached to surfaces of the samples either directly, or over thin spacers (paper stickers) glued to each contact face of the two yokes. Thickness of the applicable spacers was from zero up to 0.9 mm for the starting examination, spacers with thickness 0.08 mm and 0.23 mm were chosen as optimal for the reported measurements. Arrangement of the sample, yokes and the driving and pick-up coils are shown in Fig. 15 (left) and photo of the sample holder can be seen in Fig. 15 (right), showing a sample, the driving coil (the pick-up coil is covered by the driving one), the yokes, and a system of levers insuring a reproducible pressure of the yokes on each sample.

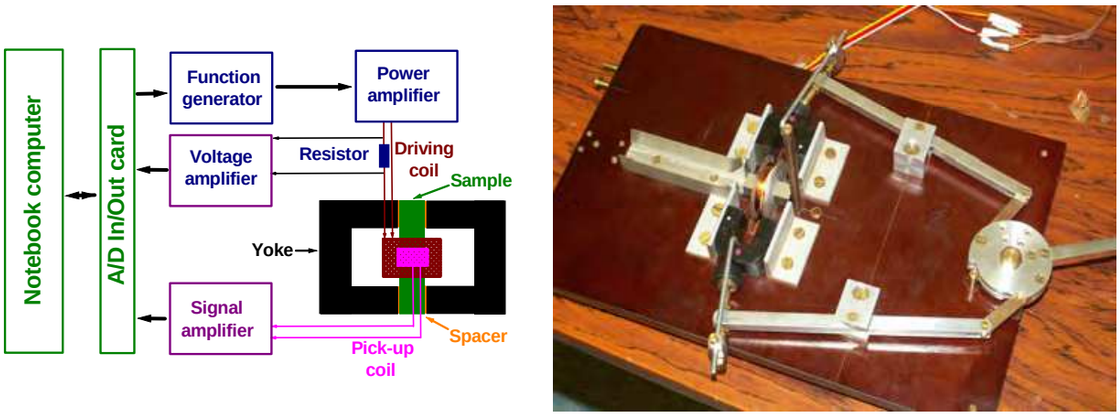

Fig. 15. Left: Sketch of the Permeameter with a magnetically open sample, coils, yokes and spacers. Right: The sample holder with the coils and the attachable yokes. The prismatic sample is placed into the coil system (by shifting it in the metal tray rightwards down to the brass stop) and the black yokes are pressed against the sample by the system of levers with the handle on the right in the picture.

The speed of change of the magnetizing current in its linear region was 1 A/s for the measurements without spacers and with spacers 0.08 mm thick, and it was 3 A/s for the measurement with the spacers 0.23 mm thick. (Increase of the speed of change of current in the latter case – as compared with the former ones – was used in order to make the signal conveniently larger.) Also the maximum amplitudes and the constant steps were different for different measurements, their applied values can be approximately read from Figs. 16a,b,c. Their choice was rather arbitrary, guided by the intention to get the sample appreciably magnetized and to fill up the range between the minimum and maximum amplitudes of the magnetizing current with a representative number of minor loops. The voltage signals measured in the pick-up coil were proportional to the effective differential permeability of the used magnetic circuits and their characteristic shapes can be seen in Fig. 16.

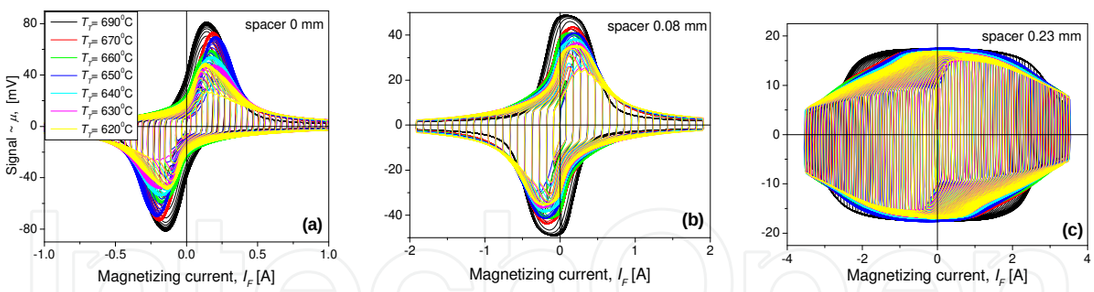

Fig. 16. (a): Measured signals from the most ductile (T_T = 690^{0}C) till the most brittle (T_T = 620^{0}C) samples, with the yokes without any spacer.
(b): Signals of the same samples measured with non-magnetic spacers 0.08 mm thick, glued on the yokes. Notice the range of the vertical axis is twice smaller and of the horizontal axis is twice larger than in figure (a).
(c): Signals of the same samples measured with non-magnetic spacers 0.23 mm thick, glued on the yokes. Notice the range of the vertical axis is four times smaller and of the horizontal axis four times larger than in figure (a).

Decision about optimum thickness of spacers can be found empirically, following measurement of peak values of signals of "good" and "bad" samples at a convenient (the same for all spacers) speed of change of the magnetizing field, using a series of available spacers. Fig. 17 shows result of such a measurement on two most ductile (T_T = 690^{0}C) samples, one with the best surfaces and the other with the worst ones. As it can be seen in Fig. 17, magnitudes of the peak values of the two samples approach each other with increasing spacer thickness. Spacers with thickness 0.08 mm and 0.23 mm were chosen as optimum ones for the illustrative measurement.

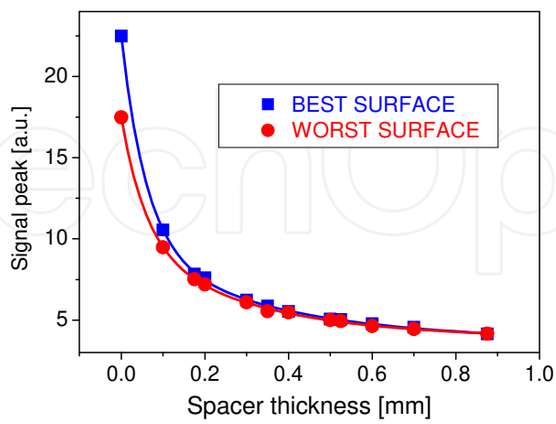

Fig. 17. Peak values of signals of two most ductile (T_T = 690^{0}C) samples, one with the best surfaces and the other with the worst ones. The two curves approach each other with increasing spacer thickness.

The optimum μ-degradation functions and the μ'_F-degradation functions for the measurement without spacer and with spacers 0.08 mm and 0.23 mm thick are plotted in Fig. 18.

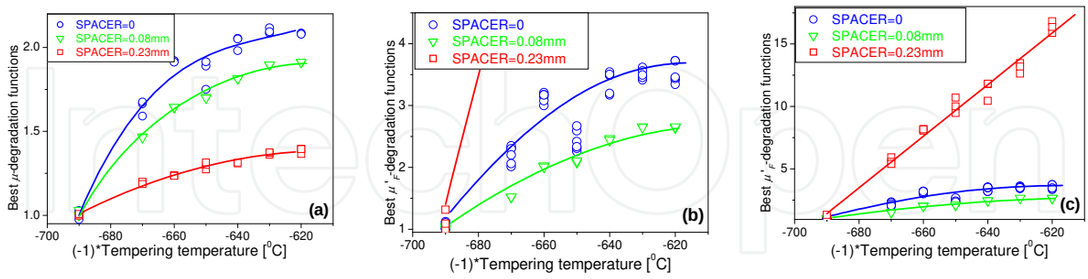

Fig. 18. (a): The best μ-degradation functions measured without any spacer (O) on the yoke faces, with spacers 0.08 mm (∇) and with spacers 0.23 mm (□).
(b): The best μ'_F-degradation functions measured without any spacer (O) on the yoke faces, with spacers 0.08 mm (∇) and with spacers 0.23 mm (□). Notice the vertical scale is doubled in comparison with figure (a).
(c): The same curves as in figure (b), just the vertical scale is four times larger than in (b).

Influence of the non-magnetic spacers inserted between the sample and the magnetically soft yokes is clearly seen in Figs. 16a,b,c: The increased distance between surface of the sample and faces of the yokes increases demagnetization within the magnetic circuits. This means a decrease of the magnetizing *field* in the sample with spacers at the use of the same magnetizing *current* as for the circuit without the spacers. However, the decreased magnetizing field fluctuates less. Beside the control of fluctuation of the magnetizing field, presence of well-defined spacers (their thickness should be found empirically by trial-and-error approach) modifies shapes of the signals measured on the series of degraded samples. Generally, with application of a spacer, substantially decreased scatter of the experimental points accompanied by a small decrease of sensitivity of the degradation functions can be expected. Such a regular behavior is presented in Figs. 18, for the μ- and the μ'_F-degradation functions measured with thin spacers (0 and 0.08 mm) in particular. A substantially thicker spacer (in our case 0.23 mm), however, is able even to modify shape of the signals considerably (see Figs. 16c), which can result in a qualitatively new shape of the degradation functions with quantitatively increased sensitivity (see Fig. 18c).

Use of the spacers for testing of material structural degradation can be recommended as a simpler alternative to more sophisticated and more demanding measurement with a direct "on-line" recording of the magnetic field at the sample surface. Especially, when it is measured by a series of field sensors and the resulting field value is obtained by extrapolation of their readings down to the sample surface, see e.g. (Stupakov, 2006, Perevertov, 2009), the outcome can be very reliable and allows compensation of fluctuating quality of the sample-yoke magnetic contact by determination of the immediate value of the magnetizing field inside the samples. Such measurements are even able of a reasonable determination of absolute magnetic parameters of the samples, which evidently cannot be done with the spacers only.

Successful use of the non-magnetic spacers can be applied for relative indication of the samples' micro-structural conditions. The spacers modify shapes of the measured signals, they substantially reduce scatter of experimental points accompanied by a slight decrease of the degradation functions sensitivity. Sometimes, thick spacers in particular, are able to modify shapes of the measured signals qualitatively and to bring about considerable increase of sensitivity, especially in the degradation functions computed from the signal derivatives. However, spacers hardly can be employed (without a simultaneous measurement of the sample surface field) for determination of purely magnetic parameters of the samples.

3.6 Temperature dependence

An important feature of any NDT technique is the permissible range of temperatures within which the method can be successfully applied. For *magnetic* methods, the tested objects are mostly ferromagnetic iron-based construction materials, namely various kinds of steel or cast iron. These materials are electrical conductors, their electric conductivity is substantially reduced not far above room temperature already, and this is the reason, why e.g. the widely successful eddy current inspections loose above room temperature a great portion of their efficiency. Not so the magnetic methods. Magnetic properties of iron-based materials do not change around the room temperature significantly yet, as they are still pretty far from their Curie point. Therefore, magnetic methods and relative magnetic NDT methods in particular, give results rather independent of temperature, if the tests are carried out within the working temperatures of most industrial objects, let us say up to about 200^0C (see Vértesy et al. 2010a).

Such behavior of MAT is demonstrated on a series of 5 ductile cast iron specimens, solidified with different cooling rates, which in its turn lead to five different microstructures with different values of Brinell hardness (see Vértesy et al. 2010b for details). MAT measurements were performed on each specimen at two different temperatures (20^0C and 180^0C) by application of an inspection head. Different rates of change ("slopes") of the magnetizing current were used. The specimens were heated by a hot plate and temperature of surface of the specimens was measured by a thermocouple. The obtained optimally chosen μ-degradation functions are shown in Fig. 19. As it can be seen there, linear

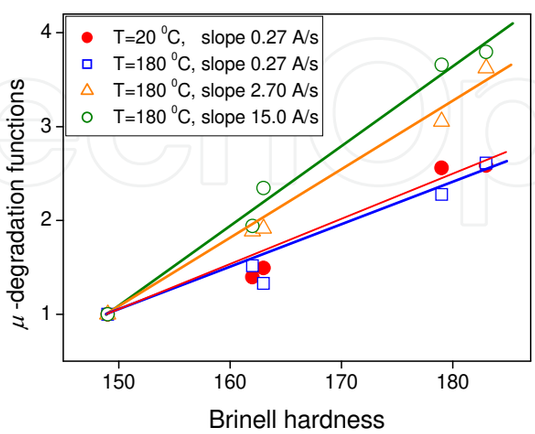

Fig. 19. The μ-degradation functions vs. the Brinell hardness measured at 20^0C and at 180^0C temperatures. Different rates of change of magnetizing current (slopes) were used in the latter case.

correlation was found between the nondestructively determined optimal μ-degradation functions and the Brinell hardness of the investigated material, and this correlation does not depend on the temperature as long as slope of the magnetizing current is kept low enough (see the red and blue lines in Fig. 19). If higher slopes are used, the influence on the μ-degradation functions is *negligible at room temperature*: the μ-degradation functions at 20^0C at rates 2.7 and 15.0 A/s coincide with the red line (not shown in Fig. 19, but kindly compare with Figs. 14a,b). At temperature 180^0C another behavior is seen: the μ-degradation functions at slopes 2.7 and 15.0 A/s increased their sensitivity with increase of the slope (see the orange and green lines).

3.7 Comparison of MAT descriptors with traditional magnetic parameters

As mentioned in Section 2, Magnetic Adaptive Testing is a magnetic hysteresis method, which – in contrast to the traditional hysteresis ones – makes use of data taken not only from the saturation-to-saturation *major* hysteresis loops of a series of degraded ferromagnetic materials, but collects information from systematically measured *families of minor* hysteresis loops. Such a large system of data is supposed to be able to completely characterize (see e.g. Preisach, 1935, Mayergoyz, 1991, Bertotti, 1998) each of the measured material, and therefore it is natural to expect it to contain also those special magnetic data, which vary with degradation of the investigated material with top sensitivity. The top-sensitive data *can* be those, utilized by the traditional hysteresis approach, but experience shows that the top sensitive data are usually different from the traditional ones.

For making a comparison between results of MAT and of a number of other widely used nondestructive magnetic methods, measurements are considered on two series of differently shaped samples of different materials plastically deformed by two different ways. The first was a series of TRIP steel magnetically open flat long bar samples (the same series as in Section 4.2.2) plastically elongated by uniaxial tension. The results of this first series are plotted in Fig. 20a. The other series were low carbon steel magnetically closed frame shaped samples (the same series as in Section 3.1) plastically compressed by cold rolling. The results of this second series are plotted in Fig. 20b. Each of the series was measured by several magnetic methods. For making the comparison possible, the results of each measurement were normalized by the corresponding value of the reference (not strained) sample. Fig. 20 shows data of the two applied ways of plastic deformation as they are reflected by the traditional major loop parameters (H_C and, $1/\mu_{MAX}$ and hysteresis losses, W), by Barkhausen noise measurement ($1/RMS$), and by the top sensitive MAT degradation functions ($1/\mu$ and $1/\mu'$). It shows that in both these illustrative cases the traditional hysteresis parameters, and also the Barkhausen data result in *qualitatively the same correlations* between the investigated magnetic characteristics and the material degradation. It is the first important conclusion of these comparative measurements, which shows in general the usefulness and equivalency of magnetic measurements.

On the other hand, this comparison clearly demonstrates that properly chosen MAT degradation functions – the $1/\mu'$-degradation functions in particular – reflect the material degradation (at least that due to plastic deformation, as shown in our example) with substantially higher sensitivity**.** *The MAT-degradation functions are typically much more*

sensitive than the traditional parameters. The evident reason for this statement is the fact, that the MAT parameters are optimized just for the investigated material and for the studied way of degradation. It is worth of mentioning that similarly good results were achieved on other materials and other ways of degradation, as well.

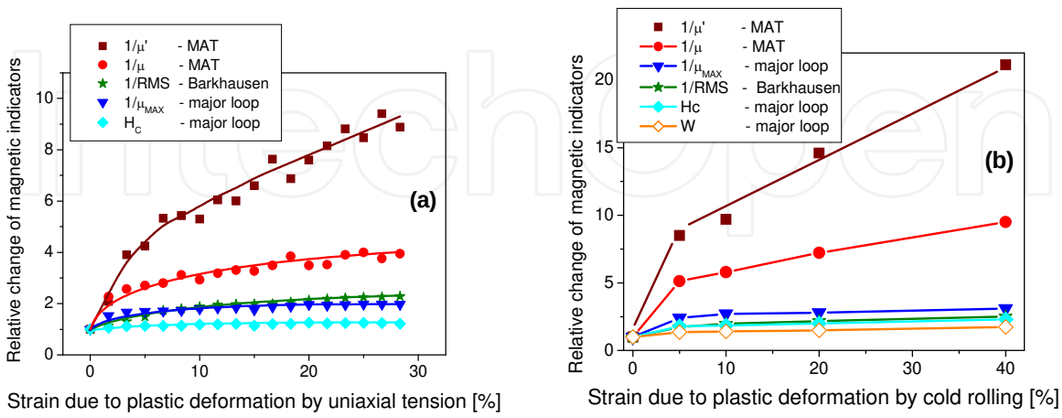

Fig. 20. Comparison of the available MAT most sensitive degradation functions picked up from the families of minor loops, with other available magnetic parameters. (a): TRIP steel *open* samples *elongated* by uniaxial tension. (b): Low carbon *closed* samples *compressed* by cold rolling.

Higher sensitivity, however, is not the single advantage of the MAT approach as compared with the traditional hysteresis and other magnetic ways of NDT. Another good point for MAT is its *multi-parametric output*, which allows not only re-check and cross-check the measured results, but in cases of non-monotonous dependencies it is often possible to use one set of data for clarification of another one, as it is shown e.g. in Section 3.3 or in (Vértesy & Tomáš, 2012). Another, experimentally very friendly feature of MAT is the fact, that there is *no need of saturation* of the measured samples. This is a very important advantage especially with magnetically open samples, where to reach saturation is usually an extremely difficult task, and the traditional methods are often forced to use minor instead of major loops anyway and just to assume the differences from the real major loops are not substantial (which is often justified, however).

Speaking about the magnetically open samples, one more interesting property must be mentioned, namely the unrestricted application of non-magnetic ***spacers*** for MAT measurement with magnetizing/sensing inspection heads or with magnetic-flux-short-cutting yokes. The point is, that for purposes and needs of MAT actually ***any magnetic value***, which can be parametrized by its field- and/or current-coordinates and which varies in a definite way with the investigated degradation of the material, is acceptable and applicable for indication of the studied degradation. Use of non-magnetic spacers brings substantial simplification of attitude and easiness of evaluation of testing, especially on samples with not ideal surfaces. See Section 3.5 and (Tomáš et al., 2012).

Last but not least, systematic measurement of the family of minor loops, with the constant rate of change of the sample magnetization in particular, makes it possible to use special ways of extrapolation for rather precise *determination of quasi-static magnitudes of magnetic*

parameters of the material even on magnetically open samples. This simple idea is thoroughly described by Ušák in his recent paper (Ušák, 2010).

4. Examples of application

4.1 Elastic deformation

Application of MAT on elastic deformation of steel samples was investigated only to a limited extent, so far. There is still plenty of space for getting experience in this field. An unpublished example is shown of a preliminary investigation of the μ-degradation functions reflecting uniaxial tension applied on a sample of Mn-Si steel (CSN 13240: Fe, 0.33-0.41%C, 1.1-1.4%Si, 1.1-1.4%Mn). Fig. 21 shows sketch of a magnetically *closed* sample shape, which made it possible to clamp the sample by its top and bottom pads into jaws of a loading machine, and to apply equal tensional stress to the two legs of the sample window. Stress-strain loading curve of the sample is shown in Fig. 22a. The magnetizing and the pick-up coils were wound on the legs and magnetization of the material was thus looped in the closed path around the sample window.

Fig. 21. Magnetically closed steel sample for testing influence of the actively applied tensional stress on the shape of the MAT degradation functions. The red rectangles show positions of the magnetizing and pick-up coils on legs of the sample window.

The result of the MAT measurement and evaluation is given in Fig. 22b. The complicated shape of the μ-degradation function reflects presence of at least three effects influencing the magnetic results: appearance of magnetic anisotropy with the pressure-induced *easy axis along* direction of the positive pressure (pulling), appearance of magnetic anisotropy with the pressure-induced reorientation of the grains in the polycrystalline material (probably reorientation of the material crystalline grains so that they get more and more oriented by their (111) axis along the direction of the pull; this should very probably induce an anisotropy with a *hard axis along* direction of the pull, and appearance of dislocations and variation of the dislocation distribution.

4.2 Plastic deformation

4.2.1 Plastic deformation of austenitic (paramagnetic) steel

4.2.1.1 Cold rolled austenitic steel

The aim of the example presented in this Section is to show application of MAT for characterization of cold rolled austenitic stainless steel specimens (Vértesy et al., 2007). Titanium stabilized austenitic stainless steel, 18/8 type, was studied. The specimens were annealed at 1100^0C for 1 hour. Then they were quenched in water in order to prevent any carbide precipitation, and to achieve homogeneous austenitic structure as the starting material. The as-prepared stainless steel specimens were cold-rolled at room temperature down to about 60% strain. The compressive plastic deformation of the material increased its

hardness and at the same time the originally paramagnetic austenite specimens became more and more ferromagnetic, due to appearance of bcc α'-martensite. Vickers hardness, *HV*, was measured destructively and nondestructive MAT measurements were performed on each specimen by attaching a magnetizing/sensing inspection head on surface of the stripe-shaped samples.

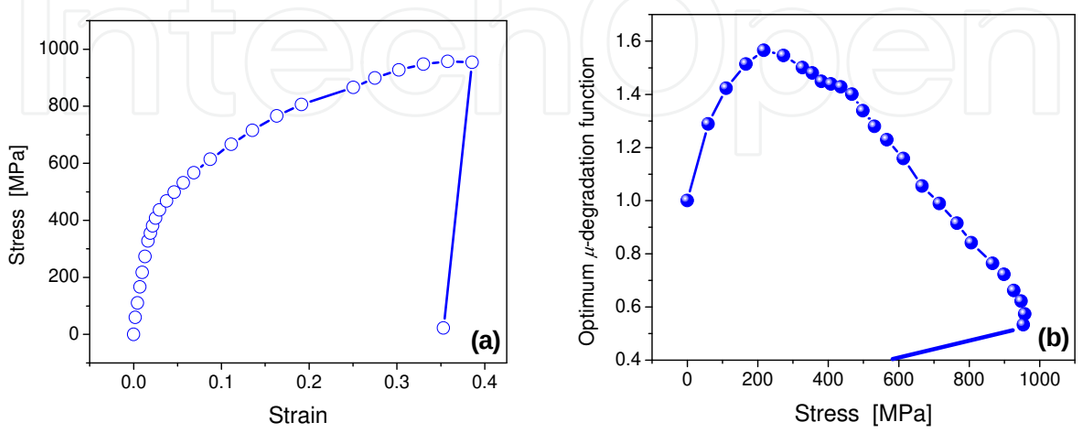

Fig. 22. (a): Stress-strain loading curve of the sample of the CSN 13240 steel, (b) The most sensitive μ-degradation function (F_i=280, A_j=560 A/m) as it depends on the applied stress. Experimental points on the two curves show stress values at which the sample was magnetized and measured.

Values of the measured Vickers hardness, *HV*, together with the most sensitive μ '-degradation function are shown in Fig. 23 in dependence on the plastic deformation strain. Evidently the MAT results offer substantially higher sensitivity and reliability of indication of the state of the stainless steel after the deformation than the traditionally used destructive hardness measurements.

4.2.1.2 Austenitic steel strained by tensile stress

Austenitic stainless steel SUS316L investigated in the present example was also plastically deformed as that in the previous Section 4.2.1.1, however this time not by compression, but by a tensile stress instead. Flat samples with original dimensions 100x70x3mm^3 were loaded up to the 50% strain. In contrast to the compressed samples, the tensile deformation did not introduce such a large percentage of the ferromagnetic phase into the deformed samples and neither the signals measured by an attached inspection head nor the μ-degradation functions gave much hope for sensitive enough magnetic indication of the strain values. However, the *B*-degradation functions (and also the μ '-degradation functions – not shown here) gave very acceptable results. The magnetic indication of the strain was substantially more efficient (up to about 30%) if the samples were magnetized along the direction of the material prolongation than normal to it (up to a few % only), as it can be seen in Fig. 24. However, it is evident, that MAT was applicable even in such an unpromising case and that it was also able to reflect anisotropy induced into the material by the stress. For more details see (Vértesy et al., 2011).

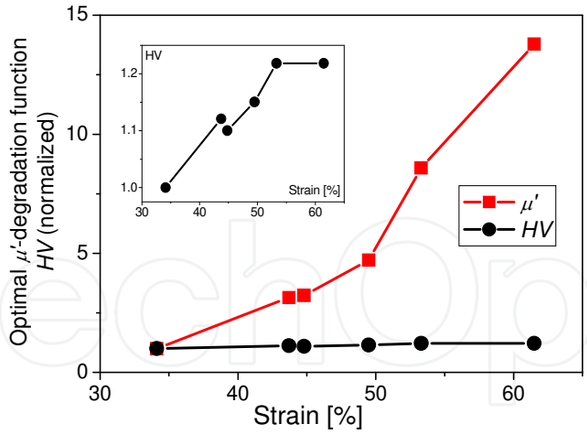

Fig. 23. The optimally chosen μ'-degradation function and the Vickers hardness, *HV*, vs. plastic strain of the samples. The inset shows the same values of *HV* but with more detailed vertical scale than that of the large plot.

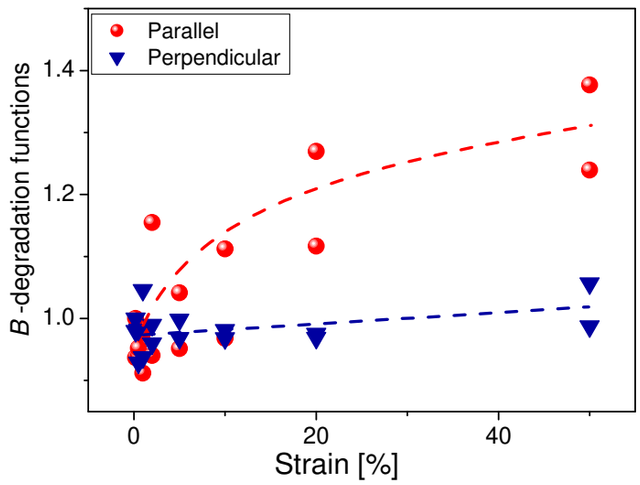

Fig. 24. The optimal *B*-degradation functions vs. residual strain of stainless steel for parallel and perpendicular magnetization with respect to the elongation.

4.2.2 Plastic deformation of ferromagnetic steel

Plastic deformation of ferromagnetic steel was investigated by MAT many times, always with excellent results. Papers (Stupakov & Tomáš, 2006, Tomáš et al., 2006, Tomáš et al., 2009a, 2009b, Vértesy et al., 2008c) and others can be quoted here, and results of a typical measurement on low carbon steel plastically deformed by uniaxial tension were used for the description of the MAT method in Section 2 and for investigation of the influence of the rate of change of the magnetizing field on sensitivity of the MAT degradation functions in Section 3.4. The results described in those two Sections are connected with the same material and similar experiments. MAT description of plastic deformation was also studied by measurements performed on magnetically open and closed samples in Section 3.1. At this place also a concise information about MAT study of a series of Transformation Induced Plasticity (TRIP) steel samples as of a specific material is added.

Transformation Induced Plasticity steels are modern materials for car industry with an excellent combination of ductility and high tensile strength. Typical mechanical parameters of TRIP materials are the upper yield strength about 540 MPa, the fracture strength about 750 MPa, and the fracture strain up to 30%. Our samples of TRIP 700 type steel with the original dimensions 150x20x1.18 mm^3 were loaded by tensile stress along their length (the production rolling direction of the material) and they were magnetized also along this direction by an attached inspection head in the MAT tests.

Eighteen samples were deformed to their relaxed strain values from 0% up to 28.33%. Vickers hardness (*HV*) measurements showed a significant increase of hardness due to the samples elongation. MAT experiments revealed a sensitive linear correspondence between the optimal μ- and μ'-degradation functions and *HV* (see Fig. 25) (and/or the strain – not presented here), and also a typical drop of the peak signal value (similar to that in Fig. 3b) between the reference (not deformed) sample and the very first deformed (with strain 1.7% only) sample. The scatter of points observed in Fig. 25 is evidently due to the untreated industrial surface of the commercial material together with application of the attached inspection head for the MAT measurement. No non-magnetic spacers (by which the scatter of points would certainly be reduced) were used in those experiments yet.

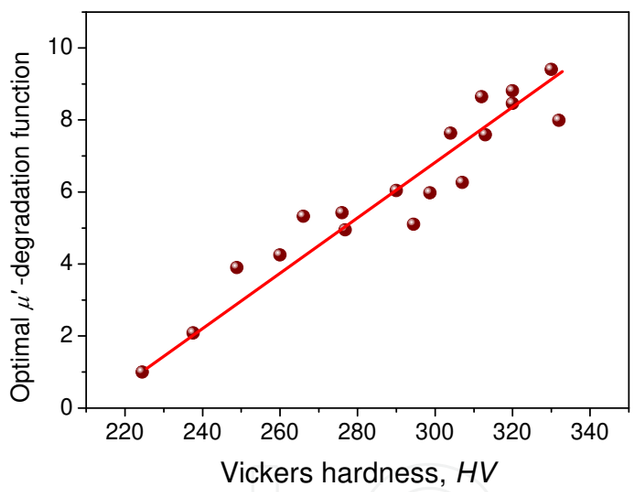

Fig. 25. The linear dependence of the optimal μ'-degradation function and Vickers hardness of the TRIP-700 steel plastically deformed by tensile loading.

4.3 Steel embrittlement

Decrease of ductility accompanied by increase of brittleness makes steel construction elements less reliable and more fault-prone. Number of processes exists, which can induce such a (usually adverse) change. Among examples of so far tested targets of MAT it is considered expedient to mention especially measurements of embrittled steel aiming at possible application of the Magnetic Adaptive Testing as a nondestructive method for checking the state of ductility/brittleness of materials used as steel coats of pressure vessels in nuclear reactors. The operational conditions of nuclear pressure vessel steel, that lead to such quality degradation include long-term bombardment by neutrons combined with intense material ageing in the elevated working temperature. As experimenting with

irradiated material requires protected environment of "hot" laboratories, first investigation of applicability of potential methods is usually performed on steel samples, which underwent *simulated not radioactive treatment* by artificial thermal ageing and artificial mechanical or thermal embrittlement.

Abilities of MAT to reflect structural modifications of thermally aged steel (Vértesy et al., 2008b), of steel embrittled by cold rolling (Vértesy et al., 2008a, Tomáš et al., 2009a, 2010) and also of steel embrittled by special thermal processing (Tomáš et al., 2011) were investigated. Only after these experiments with the not radioactive simulated materials, the measurements proceeded to irradiated pressure vessel steel in a hot laboratory. Concise information about these experiments is presented in the following text in Section 4.3.1 (embrittlement by thermal ageing), Section 4.3.2 (embrittlement by thermal processing) and Section 4.3.3 (embrittlement by neutron irradiation). Successful MAT tests of several kinds of steel embrittled by cold rolling was described in Sections 3.1, 3.7 and 4.2.1.1.

4.3.1 Steel embrittlement by thermal ageing

Cu precipitates are known to be formed in the Fe metal matrix by thermal ageing of Fe-1 wt.% Cu samples at 500^0C and these precipitates have equally large impact on mechanical properties of this material as they have in the real pressure vessel steel. Two series of this Fe-Cu alloy were annealed at 850^0C for 5 hours, followed by water quenching. Then one part of the samples was cold-rolled down to 10% deformation and isothermally aged at 500^0C for 0, 50, 500 and 5000 min. The other part of samples was aged similarly, but without the previous cold rolling (0% deformation). Vickers hardness, *HV*, of the deformed material was measured with the standard Vickers indentation technique. Then 2 mm thick ring-shaped samples were prepared having 18 mm outer and 12 mm inner diameter, respectively. The samples were equipped with a magnetizing coil and a pick-up coil each. MAT measurements were performed on those rings.

The most sensitive μ-degradation functions of the two sample series (with 10% and with 0% deformation) were determined and plotted together with the normalized Vickers hardness values in Fig. 26. The definite variation of mechanical hardness, *HV*, of the aged material testifies about the structural modifications, leading to observable change of the ductile/brittle properties. However, as it is shown in Fig. 26, MAT reflects those changes with substantially higher sensitivity than *HV* and in contrast to *HV*, MAT is monotonous. Details about the experiment and detailed discussion on the material changes can be found in (Vértesy et al., 2008b).

4.3.2 Steel embrittlement by thermal processing

One of available technologies simulating radiation embrittlement of steel is a special thermal processing described in (PHARE, 1995). At this place (see (Tomáš et al., 2011) or details) investigation by MAT is shortly presented of a large series of samples of the 15H2MFA reactor steel (widely used in nuclear plants pressure vessels VVER 440), which were artificially embrittled in this way. The magnetic measurement was accompanied by destructive Charpy impact tests done on the same samples, so that the resulting MAT degradation functions could be plotted in direct dependence on the critical ductile-brittle-transition-temperature (*DBTT*) of the material. The samples were prepared (30 pieces of

each embrittled grade) in the shape of rectangular prisms 10 x 10 x 55 mm^3, with a V-notch in the middle, applicable for the mechanical Charpy tests. However, before they were sacrificed for the mechanical destruction, they were nondestructively tested magnetically by MAT with the use of soft yokes short-cutting the magnetic flux and with nonmagnetic spacers (see Section 3.5 and Fig. 15) suppressing scatter of experimental results. The most sensitive degradation functions proved to be the $1/\mu'$- and μ'–degradation functions (as usual) and the optimal ones are plotted in Fig. 27 as functions of the *DBTT*.

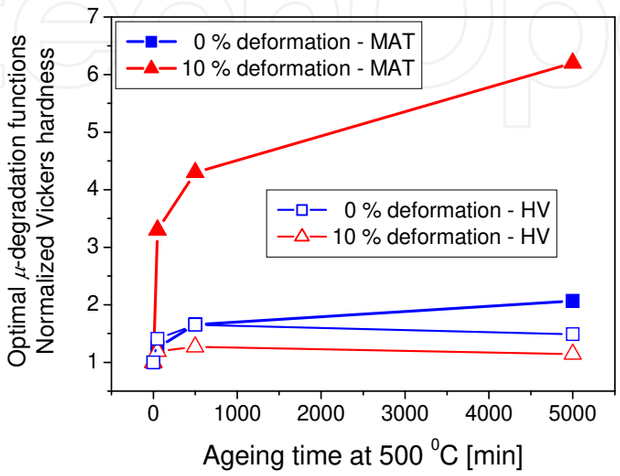

Fig. 26. The most sensitive μ-degradation functions and the averaged *normalized* Vickers hardness values of the thermally aged Fe-Cu alloy in dependence on the ageing time. The blue curves (■, □) describe the samples without previous deformation, the red ones (▲, Δ) belong to the samples compressed by 10% before start of the ageing.

MAT is shown in this Section to be sensitive enough to reflect variation of brittleness of the nuclear pressure vessel steel. It is essential, however, to keep in mind that this test of MAT on the steel, which was *embrittled by thermal processing*, reports about ability of MAT to reflect presence and density and size of *defects, which were introduced into the material* ***just and only*** *by the applied thermal processing*. The thermal processing shifted *DBTT* and Vickers hardness in this steel, but microstructure of this processed steel was certainly *different* from that of the same kind with *DBTT* shifted about the same (i.e. of the same mechanical brittleness), but embrittled by combination of the real fluence of neutrons and thermal ageing in a nuclear reactor. *The material defects after different treatments are substantially different even though the Charpy impact tests may show identical brittleness.* Magnetic Adaptive Testing is called "adaptive" just for the reason that it is able to react selectively and differently to different types of defects; it can be optimally *adapted* to them. This is considered to be one of the advantages of the method, and it was many times confirmed. Therefore, the present investigation proved MAT to "see" defects causing modification of brittleness by the thermal processing, similarly as it "saw" defects modifying brittleness of low carbon steel by cold rolling as reported in (Tomáš et al., 2009a) or in (Takahashi et al., 2006), and here in Sections 3.1 and 3.7. We can *anticipate* – by analogy – MAT to be able to see also defects caused by combination of neutron irradiation and thermal ageing, but this is all. In order to *prove* it, real experiments on irradiated/aged samples will have to be carried

out. However, magnetic "structuroscopy" and its various methods were already successfully tested at least on some irradiated samples, see e.g. (Takahashi et al., 2006, Dobman et al., 2008, Vandenbossche, 2009, Gillemot & Pirfo Barroso, 2010) and the next Section shows, that also measurements by MAT on irradiated samples were equally successful.

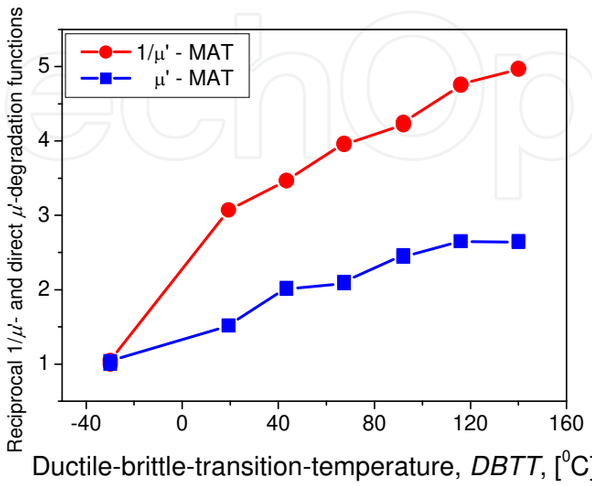

Fig. 27. Optimal reciprocal 1/μ'-degradation function and direct μ'-degradation function of the 15H2MFA nuclear pressure vessel steel embrittled by the special thermal treatment. Values of the DBTT were taken from destructive Charpy impact tests carried out on the same samples.

4.3.3 Steel embrittlement by neutron irradiation

For studying influence of neutron irradiation, block samples with dimensions 10x10x30 mm^3 were prepared from three types of nuclear reactor pressure vessel steel: JRQ is the "western", 15H2MFA is the "eastern" type reactor steel, 10ChMFT is the welding metal for steel 15H2MFA.

The samples were irradiated by neutron fluence in the $1.58x10^{19}$ – $1.19x10^{20}$ n/cm^2 range by E>1 MeV energy neutrons. (The value $1.19x10^{20}$ n/cm^2 corresponds to the neutron fluence, which a pressure vessel coat of a VVER 440 reactor obtains in approximately 20 years.) Always two samples of each material were irradiated with the same fluence, two not-irradiated ones of each material were available as reference samples. For investigation of irradiated samples by MAT technique a specially designed sample holder was built, very similar to that in Fig. 15. The samples were magnetized by a short solenoid, placed around the sample and the magnetic circuit was closed *from one side* of the sample by a passive soft magnetic yoke. A plastic dummy yoke was used from the other side, just to keep the sample fixed in the holder. Application of a *single* yoke made it possible to measure each sample independently four times from all four sides of the block. Thin non-magnetic spacers (0.08 mm) were placed between the sample and the yoke, in order to reduce fluctuation of quality of magnetic contact between the sample surface and the yoke. Measurements were performed in a protected "hot" laboratory, the samples were never touched by naked hand.

The resulting optimal MAT degradation functions are plotted in Fig. 28a for each of the three different materials. The $1/\mu$ '-degradation functions characterized the material modification the best, and very satisfactory correlation was found between the degradation functions and the neutron fluence. The type of correlation is similar for all the investigated materials: the $1/\mu$ '-degradation functions monotonously increase with increasing amount of neutron irradiation. Fig. 28b presents how *DBTT* of the 15H2MFA steel can be determined from the $1/\mu$ '-degradation function of Fig. 28a if a power law formula between the neutron fluence and *DBTT* (corresponding to typical conditions of a VVER 440 reactor) is applied for recalculation. $DBTT_0$ is the ductile-brittle transition temperature of the 15H2MFA steel before irradiation.

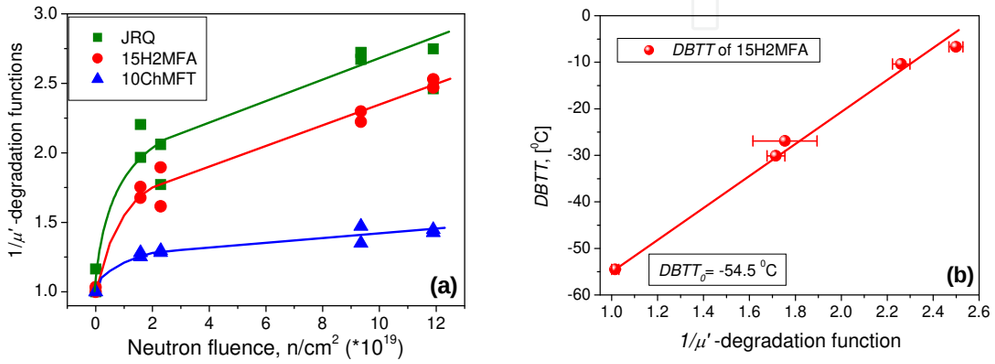

Fig. 28. (a): The optimally chosen $1/\mu$ '-degradation functions for the three investigated steels. (b): *DBTT* of the 15H2MFA steel in dependence on the $1/\mu$ '-degradation function of Fig. 28a.

In conclusion, the applicability of MAT was also demonstrated for inspection of neutron irradiation embrittlement of nuclear reactor pressure vessel steels. It should be noted at the same time, that geometry of the investigated samples was rather unfavorable for any magnetic measurement. For next measurements, and for industrial application in particular, another geometry of the samples is recommended. For instance long thin rods (e.g. 30-50 mm length and 2-3 mm diameter) could be used as surveillance samples for magnetic nondestructive tests. Such samples should be measured *contactless* in a solenoid, and much better results, not complicated by the severe problems with bad surfaces of samples having spent long periods inside a nuclear reactor, can be expected in such case.

4.4 Low cycle fatigue

Here MAT response is described to varied structures of a series of commercial steel CSN 12021 (used for high pressure pipelines), which were modified by application of low cycle fatigue. Twelve large flat steel samples were fatigued by ± cycles with the constant strain value ±0.25% and the constant strain rate of change 0.3%/s. The numbers of kilocycles (kc) applied to different samples were 0, 2, ..., 20, 22 kc. The samples would be destroyed near to 24 kc. After application of the relevant numbers of cycles, magnetically closed samples (rectangles 38x20x5 mm^3 with a hole ∅10 mm in the middle) were cut-out from the fatigued middle parts of the plates. The magnetizing and pick-up coils were wound directly on the rectangular samples through the middle hole. An optimum $1/\mu$-degradation function is presented in Fig. 29.

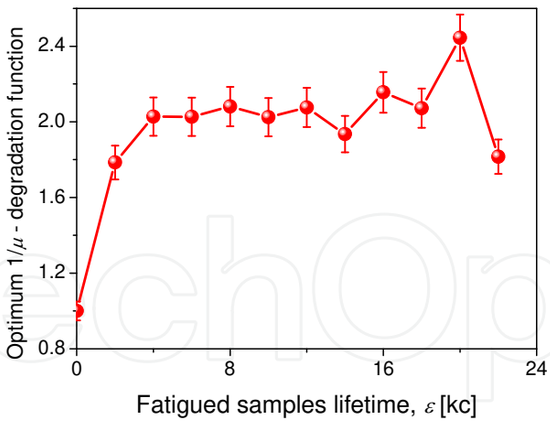

Fig. 29. The most sensitive *1/μ*-degradation function of the low cycle fatigued degraded steel. The error bars show the ±5% range, which corresponds to the scatter of magnetic properties measured on nominally identical samples of the used commercial steel.

Shape of the degradation functions (both of the *1/μ*-ones plotted here and of the *μ*-ones in (Tomáš et al., 2010) confirm the expected profile published earlier in (Lo et al., 2000), but suggesting perhaps more details and certainly more sensitivity. Magnetic reflection of the microstructure reveals radical change in the first 15% of the samples lifetime, corresponding probably to redistribution of dislocations into a volume configuration of areas with higher and lower dislocation densities, which create kind of a "cellular" pattern. In the second phase, up to about 70% of the lifetime, the situation is stabilized, which is manifested by a constant level of the degradation functions: the cellular structure of dislocation bands persists in a dynamic equilibrium with nucleation and annihilation and with some periodical shifting. During the last part of the samples lifetime, microscopical displacements of the material lead to appearance of micro-cracks, mostly at the samples surface. High local stresses at ends of the micro-cracks cause significant changes of the magnetic degradation functions again.

These last part variations of the degradation functions are the most interesting/important from the practical point of view. If indicated in time, they could serve as a warning of the approaching end of lifetime of the sample, or better of an industrial object. Shape of the degradation function in Fig. 29, suggests possible existence of such a warning. The limited number of the individual degraded samples did not allow investigation of this area in as much details as necessary within the described experiment. Behavior of the degradation functions suggests possibly even more substantial variations than in (Lo et al., 2000). The problem certainly deserves more attention and more experiments in future, with focus on the last part of the samples lifetime. Beneficial assistance of nonmagnetic spacers together with use of inspection heads on magnetically open fatigued samples should yield satisfactory results.

4.5 Decarburization of steel surface

If a steel object is exposed to normal air atmosphere at elevated temperature for an appreciable period of time, unwanted softening of the steel surface by decarburization can appear. The surface is modified into a layer of practically pure iron – the ferrite – and fatigue lifetime of such an object is dramatically shortened. Existence and also thickness of the

magnetically soft surface decarburized layer can be detected by the classical MAT approach, of course, as it can be found in (Skrbek et al., 2011). It will be shown in this Section, however, that - as suggested by (Perevertov et al., 2011) - in the case of decarburized surfaces a *modified MAT line of attack* is possible with advantage. It is based on the idea that the decarburized surface ferrite layer gets magnetically *saturated* in substantially lower applied fields than rest of the sample, and that value of the saturated magnetic flux of each ferrite layer should be proportional to its thickness. Principles and straightforward results of this MAT attitude will be shortly described here, whereas its details can be found in (Tomáš et al., 2011).

The modified MAT tests were carried out by magnetization of ring samples of carbon spring steel 54SiCr6 ($D/d/w$ = 60/54/3 mm, D – outer diameter, d – inner diameter, w – axial width). All the samples were annealed at 800^0C in air atmosphere for T = 0, 1, 4, 8, and 20 hours, respectively. A magnetizing and a pick-up coil were wound on each of the samples. The measured voltage signals of each sample were numerically integrated, and the integral at a minor loop amplitude A_j , measured on a sample annealed in air for the time-period, T, was denoted as the corresponding maximum magnetic flux $\Phi_T(A_j)$. Indicating $\Phi_0(A_j)$ such maximum magnetic flux of the reference sample, differences $(\Phi_T - \Phi_0)(A_j)$ were plotted as functions of the loop amplitudes, A_j , in Fig. 30a.

These reduced magnetic fluxes, $(\Phi_T - \Phi_0)$, of the decarburized surfaces were plotted for each loop with amplitude A_j in dependence on values of the optically measured thickness, t, of the surface ferrite (t was measured independently destructively on auxiliary samples sections). It turned out, that the plots $(\Phi_T - \Phi_0)(t)$ were very linear within surprisingly broad range of A_j. Fig. 30b gives an example of such a linear relation for the minor loop amplitude A_j = 1 kA/m, and similar linear fits were obtained in all the investigated range of the minor loop amplitudes. Fig. 30c shows the correlation coefficient, R, of such linear fits.

In conclusion it can be stated that modified MAT measurement of suitable minor hysteresis loops of ferromagnetic steel objects can serve as a fast, convenient and nondestructive method for determination of the surface decarburization level. Provided, of course, that a reference sample and at least one object of the same material, with an independently measured appreciable thickness of the decarburized layer is available so that the necessary calibration *line* can be prepared. Range of the appropriate minor loop magnetizing amplitudes was shown to be broad, the measurement simple and not requiring any sophisticated equipment.

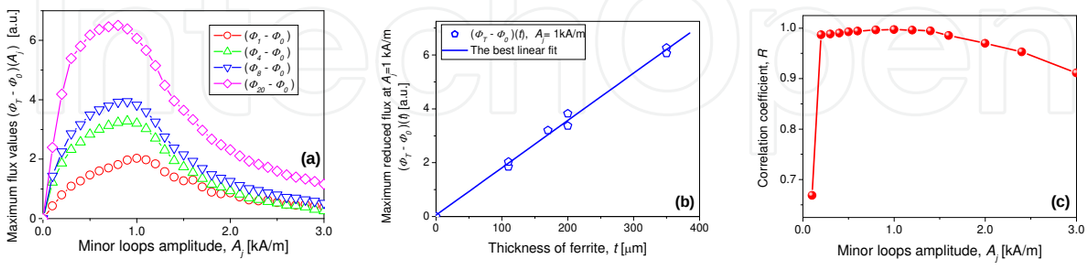

Fig. 30. (a): The maximum magnetic flux values of the samples reduced by the maximum flux value of the reference sample, $(\Phi_T - \Phi_0)(A_j)$, at minor loops with amplitudes A_j. (b): The reduced maximum magnetic flux values, $(\Phi_T - \Phi_0)$, of the air-annealed samples, at the minor loop with amplitude A_j=1 kA/m, as a function of thickness, t, of the surface decarburized ferrite. (c): Correlation coefficient, R, of the linear regression fit with $(\Phi_T - \Phi_0)(t)$, for the used range of the minor loop amplitudes, A_j.

4.6 Welding quality tests

Point welding is a frequently used technology in industry, and checking quality of welding is very important. Welding process produces serious phase transformation in the welded area of the material, which is accompanied by modification of magnetic characteristics. It is shown in this Section how MAT can be applied for inspection of point welding of car-body sheets.

Thickness of the point-welded sheets was 1.2 mm, the material was cold rolled low carbon steel. Two series of welded points were produced by 2.4 bar pressure welding and the welding current was modified from 15.6 up to 21.8 kA. Diameter of the welded points was around 7 mm. A MAT-checked row of welded points is shown at the bottom of Fig. 31a, a destructively tested control series of welded points can be seen at the top of Fig. 31a. Result of the destructive tests confirmed, that welded points made by the welding current between 18.5 and 20 kA were proper. The points with lower current were not welded strongly enough, the points above 20 kA were over-welded (over-welding damaged the material).

MAT measurements were performed on each welded point with a magnetizing yoke. The result of the measurement is shown in Fig. 31b, where the optimally chosen $1/\mu$-degradation function vs. the welding current can be seen. It is worth to mention, that even a small change of the welding current results in a measurable modification of the MAT degradation functions at the beginning of the curve, and this becomes more pronounced in the critical region from 18.5 to 20 kA. All the MAT degradation functions were normalized by the corresponding value of a reference spot (where no welding was taken). More than 100% difference was found between the MAT degradation functions corresponding to the lowest and to the highest energy of welding, which makes possible to characterize quality of the welding quite easily.

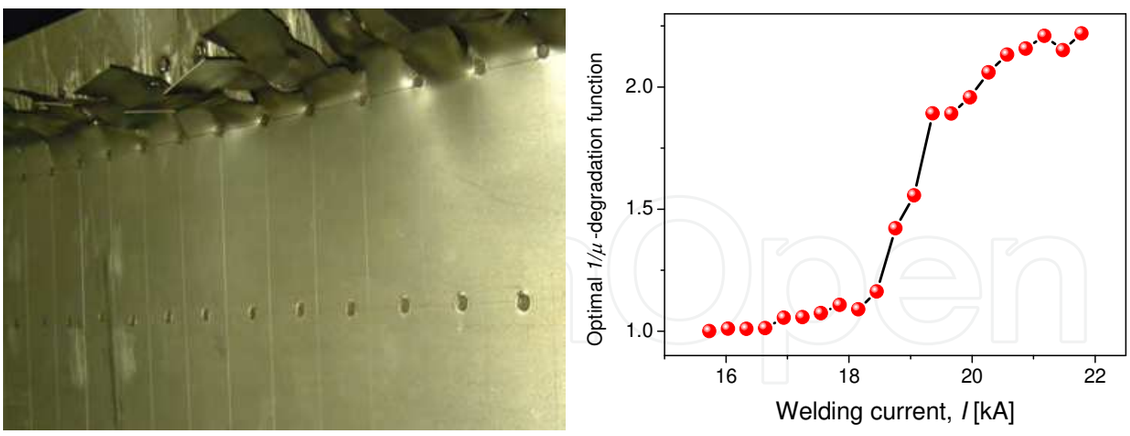

Fig. 31. (a): Two rows of welded points, each produced by a different welding current. The upper row shows results of the destructive test. (b): The optimally chosen $1/\mu$-degradation function vs. the welding current, measured on the bottom row of welded points shown in figure (a).

Choice of the optimal degradation functions is not critical, the top sensitivity area of $1/\mu$-degradation functions in the sensitivity map is very large. For the next possible industrial application also tolerance towards of the results with respect to exact positioning of the

magnetizing yoke was investigated. The same welded spot was measured several times after each other, the position of the yoke with respect to the welded spot was modified, and MAT evaluation was performed. The results are seen in Fig. 32, where three characteristic cases are shown. In the left case the welded spot was in the central area of the yoke, in the middle case only half area of the welded spot was under the yoke, and in the right case the welded spot was completely outside. The figure shows how the $1/\mu$-degradation functions values were changing compared with the central position of the yoke. Even the most unfavorable case caused 3% difference in the MAT degradation function value only.

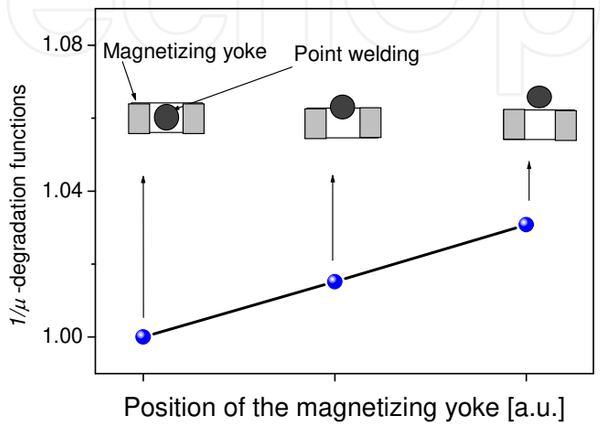

Fig. 32. Variation of the MAT $1/\mu$-degradation functions, if the measurement was performed on the same welded spot at three characteristic positions of the yoke with respect to the welded spot, as indicated in the figure.

4.7 Search for flaws

Detection and evaluation of thickness reduction of pipes are very important issues for prediction of lifetime of pipelines in order to avoid severe accidents (Ju, 2007). Recently many nondestructive testing techniques have been used for the measurement of pipe wall thinning, but none of them gives satisfactory result in the case of ferromagnetic carbon steels, especially if the steel is thick or if it is *layered*. In this Section it is shown how Magnetic Adaptive Testing can be applied for inspection of wall thinning in layered ferromagnetic materials. Experiments were performed on a system of ferromagnetic carbon steel plates, one of them containing an artificial slot (see also (Vértesy et al., 2012b)).

Preliminary experiments verified, that samples with different total thickness give different signals from the MAT inspection head. Evidently similar modifications of the signal can be expected if thickness of the sample or of one of the layered samples is modified only locally. It was simulated by three plates (180x170x3 mm^3) made of a carbon steel, with one of them containing a 9x2 mm^2 slot in the middle. Fig. 33 shows the case if all the three sheets are put together. The samples were measured in such a way, that they were magnetized by an inspection head from the top side, while the slot was placed at the bottom. The measurements were performed on both "double" and "triple" configurations (Fig. 34), and the head was attached in both parallel and perpendicular orientations with respect to the axis of the slot. The head was moved on the top sample surface along a direction perpendicular to the axis of the slot. Distance, x, of the center of the head from the middle of

the slot was the independent parameter. In this case cross-section of the magnetic yoke of the inspection head was 10.5x16 mm², the total outside length 31 mm, and the total outside height of the bow 31 mm. The distance between the legs was 10 mm.

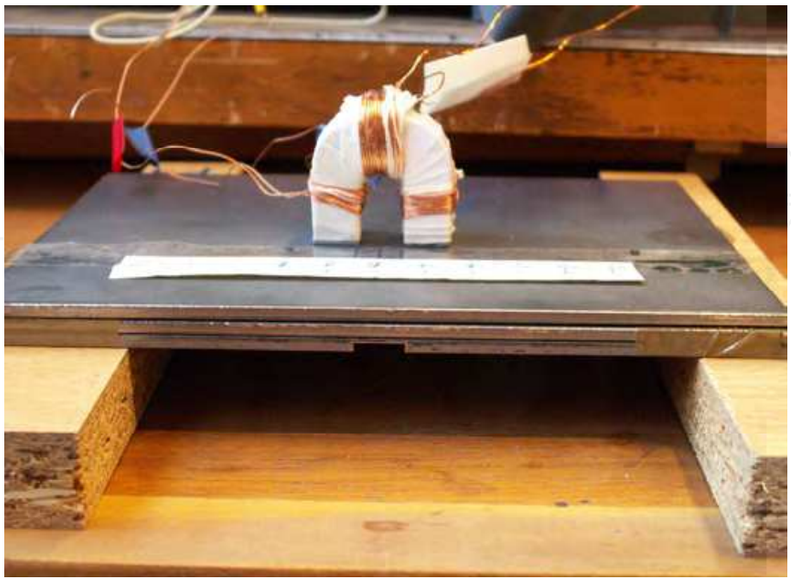

Fig. 33. Measurement of the triple sheet with perpendicular orientation of the yoke.

Results of the measurements, performed on the double sheet system and sketch of the experimental arrangement are shown in Fig. 34a. The yoke was oriented perpendicular to the axis of the slot in this case. The optimally chosen μ-degradation functions were normalized by the value, measured at the largest distance from the center of the slot (x = - 60 mm). A very similar result was obtained if the yoke was oriented parallel with the slot axis and moved similarly as in the former case. The measurement was performed in a triple sheet configuration, too, with the results shown in Fig. 34b. The experiments revealed that Magnetic Adaptive Testing is a promising tool for nondestructive detection of thinning of steel slabs from the other side of the specimen, and that it is able to give good results even for a layered ferromagnetic material.

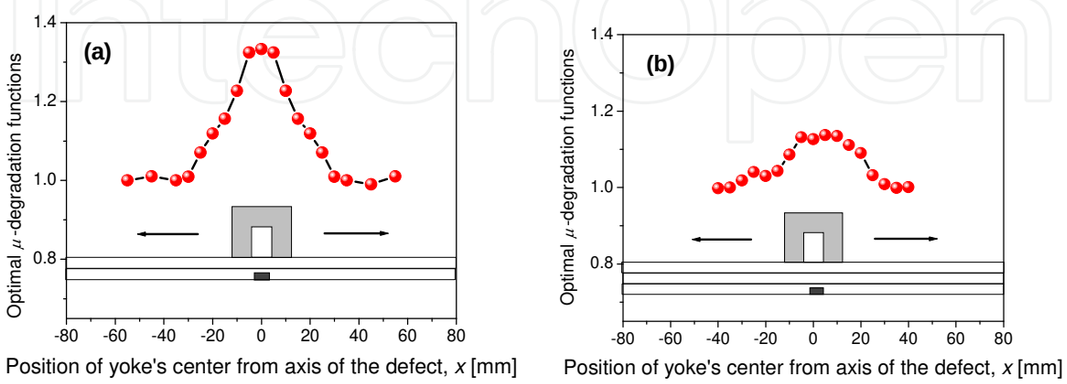

Fig. 34. Optimal MAT degradation functions in dependence on the inspection head position for perpendicular configuration in a (a) double sheet system, (b) triple sheet system.

4.8 Cast iron

4.8.1 Ductile cast iron

Special series of ductile cast iron samples was investigated (see also (Vértesy et al., 2010c)) Staircase-shaped samples were prepared, where different cooling rates resulted in different structures. Correlations were studied of the *nondestructively* measured MAT degradation functions with the *destructively* determined Brinell hardness and also with the electrical conductivity of the samples. Four staircase-shaped block specimens with 5 steps each were prepared. (One of these samples was used here earlier for temperature dependence investigations, see Section 3.6.) Chemical composition of the cast iron samples is shown in Table 1. The amount of ferrosilicon and of commercial pure iron in the melt was controlled, in order to get different carbon equivalents. The targeted carbon equivalent of sample 1 was set to a low value, in order to have cementite in the matrix. The targeted chemical compositions of samples 2, 3 and 4 were the same, but they were given different heat treatments, in order to have different matrices.

Sample	C	Si	Mn	P	S	Mg
1	3.05	2.041	0.166	0.049	0.016	0.024
2	3.58	2.592	0.127	0.065	0.016	0.025
3	3.46	2.575	0.128	0.066	0.015	0.025
4	3.43	2.523	0.130	0.064	0.016	0.026

Table 1. Chemical composition of the ductile cast iron samples (values in wt%).

These staircase-shaped block specimens were used for magnetic measurement: each step was measured. The samples were magnetized by a magnetizing inspection head, attached on the surface. The optimally chosen *B*-degradation functions of the samples are shown in Fig. 35 in dependence on the Brinell hardness and on the electric conductivity. All the steps of all the measured (four) samples are taken into account within this figure. (Fig. 19 in Section 3.6 shows the dependence of a μ-degradation function on the hardness for sample 4.) The degradation function values of different samples were normalized by the sample with the lowest hardness.

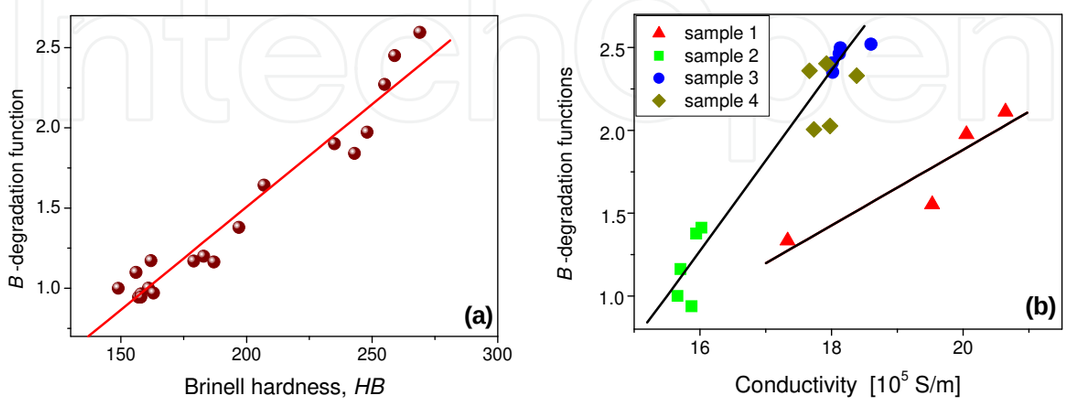

Fig. 35. The most sensitive *B*-degradation functions in dependence on Brinell hardness (a) and on conductivity (b).

The Brinell hardness and the MAT degradation functions correspond to each other very well, linear correlation was found. It should be emphasized that the presented relationship was obtained when *all* the samples (with different chemical compositions and preparation conditions) were considered for the evaluation. (Considering the steps within each single sample, the scatter of points is significantly smaller, as shown in Fig. 19). In any case the reliability and reproducibility of the MAT degradation functions are good, as determined from the sensitivity maps. A good correlation was also found between the MAT degradation functions and conductivity, but in this case the samples with different chemical composition should be handled separately, as can be seen in Fig. 35b. The optimally chosen MAT degradation functions of samples 2, 3 and 4, which have rather similar compositions, lie more-or-less on a straight line as a function of conductivity. This is also valid for sample 1, but with a different slope.

4.8.2 Flake graphite cast iron

Flake graphite cast iron materials with various graphite structures and matrices were prepared and their magnetic properties were measured and evaluated systematically. Correlation of the *nondestructively* measured MAT parameters has been studied with the *destructively* determined Brinell hardness, the pearlite/ferrite ratio and the graphite morphology. Three flake graphite cast iron materials with different chemical compositions listed in Table 2 were prepared. Disks, prepared of these materials were subjected to two kinds of heat treatment: annealing (AN) to obtain a *ferrite-based* matrix and normalization (NR) to obtain a *pearlite-based* matrix. To treat these annealed and normalized disks, they were heated at 1123 K in a furnace for one hour and then either cooled in the furnace or in air for AN and NR, respectively. Altogether 9 flake graphite cast iron materials with various matrices and graphite shapes were thus produced. After grinding the specimen surfaces, their Brinell hardness, *HB,* was measured confirming that the normalizing and annealing treatments were successful in producing the fully ferritic and fully pearlitic matrices, respectively. Metallographic examination also revealed, that the as-cast samples (samples without the heat treatments) had differently mixed pearlite/ferrite matrices.

Material	Chemical composition (mass%)						
	C	Si	Mn	P	S	Cr	Ti
CE4.7	3.77	2.78	0.78	0.025	0.015	0.029	0.015
CE4.1	3.36	2.15	0.69	0.018	0.010	0.014	0.011
CE3.7	3.13	1.66	0.72	0.017	0.020	0.038	0.010

Table 2. Chemical composition of flake graphite cast iron samples (values in wt%).

The samples were magnetized by an attached inspection head for the MAT investigation and degradation functions of all the investigated samples were evaluated. The optimal $1/\mu$-degradation functions are plotted against the Brinell hardness in Fig. 36.

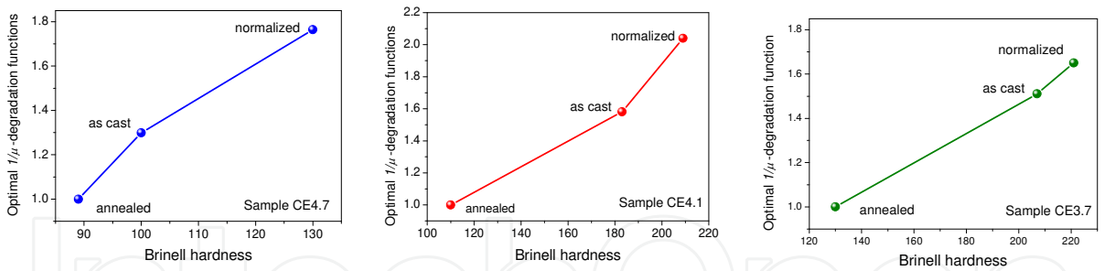

Fig. 36. Optimally chosen $1/\mu$ -degradation functions of the sample series CE4.7, CE4.1 and CE3.7 vs. Brinell hardness.

The applied annealing resulted in completely ferrite-based matrices (the 0% pearlite/ferrite ratio) and the normalization resulted in completely pearlite-based ones (the 0% pearlite/ferrite ratio). The pearlite/ferrite ratio of the as-cast samples was different for different sample series, and it was determined by metallographic examination. The pearlite/ferrite ratio and the average length of graphite flakes were evaluated using an image processing software. Correlation between the optimal $1/\mu$-degradation function and the pearlite/ferrite ratios is given in Fig. 37.

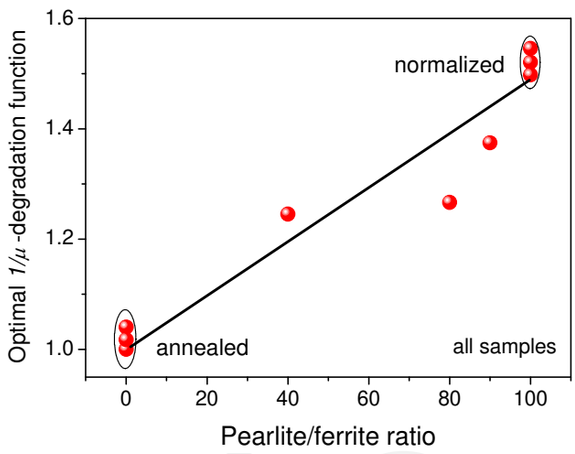

Fig. 37. Optimally chosen $1/\mu$-degradation function of all the samples vs. perlite/ferrite ratio. The annealed and the normalized samples are indicated.

Graphite area and graphite length characterize the graphite structure of the investigated samples. MAT degradation functions were evaluated as functions of these quantities for the three as-cast samples, and the corresponding values were compared with each other. Correlation between the magnetic parameters and the graphite area can be seen in Fig. 38a, while correlation between the magnetic parameters and the graphite length is plotted in Fig. 38b.

Concluding the observations, closely linear correlation was found between the MAT degradation functions and the Brinell hardness. It is valid if influence of the heat treatments was investigated within the series of samples with the same chemical composition (as shown in Fig. 36), but also if influence of chemical composition was studied for different as-cast samples, and also if even all the samples were considered within the same graph (these

last two cases are not shown here). This confirms the expectation that magnetic hardening correlates with the mechanical hardening of cast iron very well. This is why MAT is also an excellent tool for determining the pearlite/ferrite ratio. Degradation functions of all 0% pearlite/ferrite ratio samples are very close to each other, the difference is not larger than the error of measurement, and the same holds for the normalized samples (100% pearlite/ferrite ratio case). The difference of about 50% in magnitude of the shown $1/\mu$-degradation function is more than enough for determination of variations between the pearlite/ferrite ratios from 0% to 100% (see Fig. 37). The larger scatter in Fig. 37 of the degradation functions evaluated on the as-cast samples can be probably attributed to inaccurate determination of the pearlite/ferrite ratio, which was rather estimated from microphotographs of their structure. MAT was also found to be a useful tool for measurement of parameters of graphite morphology. Very satisfactory linear correlation between optimally chosen MAT degradation functions and both the graphite length and the graphite area was found on the as-cast samples in Fig.38. The correlation between MAT degradation functions and the graphite morphology is evident even if all the samples are considered, however in this case the scatter of points is larger.

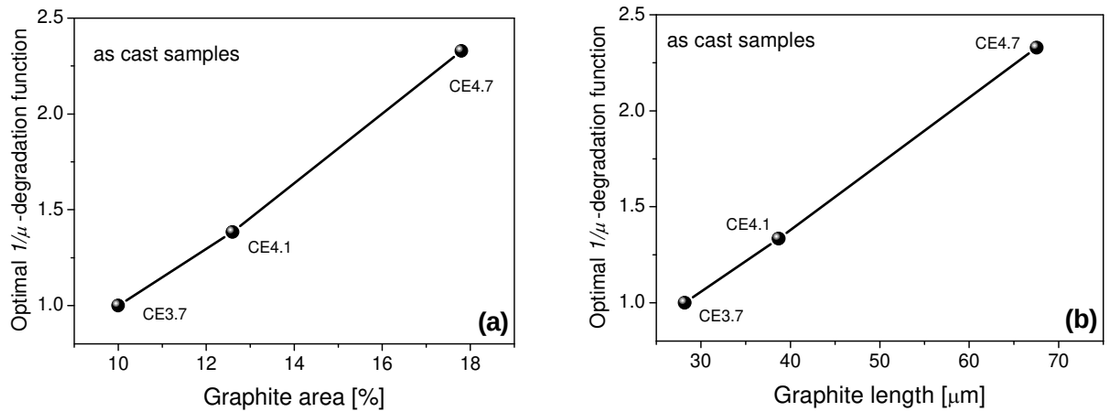

Fig. 38. Optimally chosen $1/\mu$-degradation functions of the as-cast samples vs. the graphite area (a) and vs. the graphite length (b).

5. Conclusions

An original magnetic nondestructive method of Magnetic Adaptive Testing is presented in this chapter as a sensitive option to other ways of investigation of modification of properties of ferromagnetic construction materials. Physical basis, principles and ways of application of the method are explained in the first and second Sections, suggestions with respect to its efficient use are given in Section 3, and Section 4 is dedicated to several examples of measurements, where MAT was utilized, usually with very satisfactory results.

MAT belongs to the family of nondestructive *magnetic hysteresis* material testing methods, which generally investigate structural modifications of *bulk* of the tested objects, and it is shown to *surpass sensitivity* of the traditional hysteresis methods mainly due to its specific selection from the recorded large data-pool of that part of information, which is *optimal with respect to the investigated material and to the way of its degradation*.

The most advantageous features of Magnetic Adaptive Testing were demonstrated through many successful measurements on many different materials, which underwent different types of degradation (fatigue, annealing, plastic deformation, neutron irradiation, etc.). MAT generally offers significantly larger sensitivity – with respect to any degradation parameter – than any of other magnetic nondestructive and probably even of any existing destructive method. A very important, advantageous feature of the MAT technique is that it *does not require magnetic saturation* of investigated samples. The most appropriate MAT descriptors of each type of degradation are chosen from a big data-pool, and this multi-parametric choice frequently makes possible to characterize the material degradation in a more complex way, than other methods. It was also shown that the optimally chosen degradation functions are reliable and repeatable. Magnetic Adaptive Testing is a comparative measurement, it does not offer any absolute magnetic quantities. Inspection of any unknown sample is based on a previous "teaching" process.

The most serious drawback of this technique is that in great majority of practical applications the MAT inspection is required to operate on magnetically open industrial objects, where shape of the object (through the demagnetization factor) and condition of its surface can introduce uncertainty into the measurement. However, it was shown that qualitatively the same correlation exists between the MAT degradation functions and the degradation variables both for open and for closed magnetic circuits (Section 3.1, and/or 3.2), and also that the surface problem can be treated rather successfully (Section 3.5).

Main directions promising to contribute to further development of the MAT application are probably a next improvement of MAT inspection heads for contact measurement on surfaces of industrially interesting objects, namely in finding a satisfactory elimination of fluctuation of quality of magnetic contact between the inspection head and surface of the object, which is frequently uneven, rough and deteriorated. An important step in this direction was achieved by application of non-magnetic spacers, which was described in Section 3.5 and successfully applied in several latest measurements. Perhaps a *simple* measurement of a parameter proportional to the real value of the magnetizing field inside the object magnetized from its surface could do the trick.

As for the most promising next industrial application of MAT, the nondestructive surveillance program for irradiated steel of nuclear pressure vessel reactor steel (Section 4.3.3) should be pointed out, and quantitative measurement of steel surface decarburization (Section 4.5). Probably also fatigue tests of periodically loaded objects could give very well applicable results, which, however, still require broad next experimental study, substantially more detailed than the first attempt mentioned in Section 4.4.

6. Acknowledgements

The authors if this chapter would like to express their gratitude to all the colleagues, who were co-authors of the quoted papers and also to those who took part at preparation of the presented experiments. Special thanks aim at the members of the Universal Network for Magnetic Nondestructive Evaluation, the annual workshops of which made a very fruitful and supporting platform for discussions and inspiration. The work was financially supported by the Czech Institute of Physics, v.v.i. of ASCR (project AVOZ 10100520) and by the Hungarian Research Institute for Technical Physics and Materials Science of HAS, by the

Hungarian-Czech and by the Hungarian-Japanese Bilateral Intergovernmental S&T Cooperation projects, by the project No.101/09/1323 of the Grant Agency of the Czech Republic, and by the Hungarian Scientific Research Fund (projects T-035264, K-62466 and A08 CK 80173).

7. References

Bertotti G. (1998) *Hysteresis in Magnetism*, Academic Press, San Diego

Blitz J. (1991) *Electrical and Magnetic Methods of Nondestructive Testing*, Adam Hilger IOP Publishing, Ltd, Bristol

Devine M.K. (1992) Magnetic detection of material properties (1992) *J. Min. Met. Mater. (JOM),* pp. 24-30

Devine M.K., Kaminski D.A., Sipahi L.B. Jiles D.C. (1992) Detection of fatigue in structural steels by magnetic property measurements, Journal of Materials Engineering and Performance, Vol. 1, pp. 249-253

Dobmann G., Altpeter I., Kopp M., Rabung M., Hubschen G. (2008) ND-materials characterization of neutron induced embrittlement in German nuclear reactor pressure vessel material by micromagnetic NDT techniques, *Electromagnetic Nondestructive Evaluation (XI),* p.54, IOS Press, ISBN 978-1-58603-896-0

Gillemot F., Pirfo Barroso S. (2010) Possibilities and difficulties of the NDE evaluation of irradiation degradation, *Proceedings of 8th International Conference on Barkhausen Noise and Micromagnetic Testing (ICBM8)* (ISBN 978-952-67247-2-0)

Jiles D.C. (1988) Review of magnetic methods for nondestructive evaluation, *NDT International* Vol. 21, p. 311

Jiles D.C. (2001) Magnetic methods in nondestructive testing, In: *Encyclopedia of Materials Science and Technology,* K.H.J. Buschow et al., Eds, p.6021, Elsevier Press, Oxford

Ju, Y. (2007) Remote measurement of pipe wall thinning by microwaves, *Advanced Nondestructive Evaluation II,* Volume 2 pp. 1128-1133

Lo C.C.H., Tang F., Biner S.B., Jiles D.C. (2000) Effects of fatigue-induced changes in microstructure and stress on domain structure and magnetic properties of Fe-C alloys, *J. Appl. Phys.*, Vol. 87, p. 6520

Mayergoyz I.D. (1991) *Mathematical Models of Hysteresis*, Springer-Verlag, Berlin PHARE PH2.01/95 Project "Reactor Pressure Vessel" 1995

Preisach F. (1935) Uber die magnetische Nachwirkung, *Zeit. fur Physik* Vol. 94 p. 277

Perevertov O. (2009) Increase of precision of surface magnetic field measurements by magnetic shielding, *Meas. Sci. Technol.*, Vol. 20, p. 055107

Perevertov O., Stupakov O., Tomáš I., Skrbek B. (2011) Detection of spring steel surface decarburatization by magnetic hysteresis measurements, *NDT&E International* Vol. 44 pp. 490–494

Skrbek B., Tomáš I., Kadlecová J., Ganev N. (2011) NDT Characterization of Decarburization of Steel after Long-Time Annealing, *Kovove Materialy – Metallic Materials*, Vol. 49, No.6, pp.401-409

Stupakov O. (2006) Investigation of applicability of extrapolation method for sample field determination in single-yoke measuring setup, *J. Magn. Magn. Mater.* Vol. 307 pp. 279-287

Stupakov O., Tomáš I., Kadlecová J. (2006) Optimization of single-yoke magnetic testing by surface fields measurement, *J.Phys. D* Vol. 39, pp. 248-254

Stupakov O., Tomáš I. (2006) Hysteresis minor loop analysis of plastically deformed low-carbon steel, *NDT&E Int.* Vol. 39 pp. 554-561

Takahashi S., Kobayashi S., Kikuchi H., Kamada Y. (2006) Relationship between mechanical and magnetic properties in cold rolled low carbon steel, *J. Appl. Phys*., Vol. 100, p.113908

Takahashi S., Kikuchi H., Ara K., Ebine N., Kamada Y., Kobayashi S., Suzuki M. (2006) In situ magnetic measurements under neutron radiation in Fe metal and low carbon steel, *J. Appl. Phys.* Vol. 100, p.023902

Tomáš I. (2004) Non-Destructive Magnetic Adaptive Testing of Ferromagnetic Materials, *J. Magn .Magn. Mater.* Vol. 268/1-2, pp. 178-185

Tomáš I., Stupakov O., Kadlecová J., Perevertov O. (2006) Magnetic Adaptive Testing – low magnetization, high sensitivity assessment of material modifications, *J. Magn. Magn. Mater*. Vol. 304 pp.168-171

Tomáš I., Vértesy G., Kobayashi S., Kadlecová J., Stupakov O. (2009a) Low-carbon steel samples deformed by cold rolling – analysis by the magnetic adaptive testing, *J. Magn. Magn. Mater.*, Vol. 321 pp. 2670-2676

Tomáš I., Vértesy G., Kadlecová J. (2009b) Influence of rate of change of magnetization processes on sensitivity of Magnetic Adaptive Testing, *J. Magn. Magn. Mater*. Vol. 321 pp. 1019-1024

Tomáš I., Vértesy G., Kadlecová J. (2009c) Influence of rate of change of magnetization processes on sensitivity of Magnetic Adaptive Testing, *J.Magn. Magn. Mater.* Vol. 321 pp. 1019-1024

Tomáš I., Kadlecová J., Vértesy G., Skrbek B. (2010) Investigation of Structural Modifications in Ferromagnetic Materials by Magnetic Adaptive Testing, *Proceedings of 8th International Conference on Barkhausen Noise and Micromagnetic Testing (ICBM8)*, pp.153-162 (ISBN 978-952-67247-2-0)

Tomáš I., Kadlecová J., Konop R., Dvořáková M. (2011) Magnetic nondestructive indication of varied brittleness of 15Ch2MFA steel, *Proceedings of 9th International Conference on Barkhausen Noise and Micromagnetic Testing (ICBM9)* ISBN 978-952-67247-4-4 (paperback), ISBN 978-952-67247-5-1 (CD-ROM), pp. 55-63

Tomáš I., Kadlecová J., Vértesy G. (2012) Measurement of flat samples with rough surfaces by Magnetic Adaptive Testing, *IEEE Trans. Magn*., in press

Ušák E. (2010) A new approach to the evaluation of magnetic parameters for non-destructive inspection of steel degradation, *Journal of Electrical Engineering*, Vol. 61. pp. 100-103

Vandenbossche L. (2009) Magnetic Hysteretic Characterization of Ferromagnetic Materials with Objectives towards Non-Destructive Evaluation of Material Degradation, Gent University, Gent, Belgium, PhD Thesis

Vértesy G., Tomáš I., Mészáros I. (2007) Nondestructive indication of plastic deformation of cold-rolled stainless steel by magnetic adaptive testing, *J. Magn. Magn. Mater*. Vol. 310 pp. 76-82

Vértesy G., Tomáš I., Takahashi S., Kobayashi S., Kamada Y., Kikuchi H. (2008a) Inspection of steel degradation by Magnetic Adaptive Testing, NDT & E INTERNATIONAL, Vol. 41. pp. 252-257

Vértesy G., Tomáš I., Kobayashi S., Kamada Y. (2008b) Investigation of thermally aged samples by Magnetic Adaptive Testing, *Journal of Electrical Engineering*, Vol. 59. pp.82-85

Vértesy G., Tomáš I., Takahashi S., Kobayashi S, Kamada Y, Kikuchi H., (2008c) Inspection of steel degradation by Magnetic Adaptive Testing, NDT & E INTERNATIONAL, Vol. 41. pp. 252-257

Vértesy G., Uchimoto T. Tomáš I., Takagi T. (2010a) Temperature dependence of magnetic descriptors of Magnetic Adaptive Testing, *IEEE Trans..Magn.*, Vol. 46. pp. 509-512

Vértesy G., Uchimoto T. Tomáš I., Takagi T. (2010b) Nondestructive characterization of ductile cast iron by Magnetic Adaptive Testing, *J. Magn. Magn. Mater.* Vol. 322 pp. 3117-3121

Vértesy G., Uchimoto T., Takagi T., Tomáš I. (2010c) Nondestructive inspection of ductile cast iron by measurement of minor magnetic hysteresis loops, *Materials Science Forum*, Vol. 659. pp. 355-360

Vértesy G., Ueda S., Uchimoto T., Takagi T., Tomáš I., Vértesy Z. (2011) Evaluation of Plastic Deformation in Steels by Magnetic Hysteresis Measurements, In: *Electromagnetic Nondestructive Evaluation (XIV)*, T. Chady et. al., Eds., pp. 371-378, IOS Press, Amsterdam

Vértesy G., Tomáš I. (2012a) Complex characterization of degradation of ferromagnetic materials by Magnetic Adaptive Testing, *IEEE Trans. Magn.*, in press

Vértesy G., Tomáš I. Uchimoto T., Takagi T. (2012b) Nondestructive investigation of wall thinning in layered ferromagnetic material by magnetic adaptive testing, NDT & E INTERNATIONAL, Vol 47. pp. 51-55

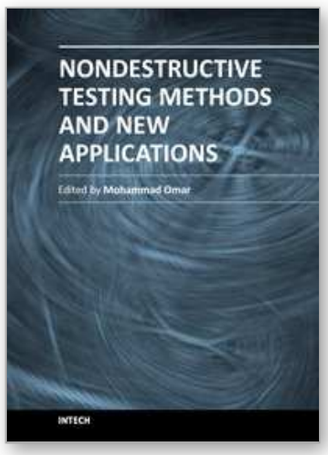

Nondestructive Testing Methods and New Applications

Edited by Dr. Mohammad Omar

ISBN 978-953-51-0108-6
Hard cover, 264 pages
Publisher InTech
Published online 02, March, 2012
Published in print edition March, 2012

Nondestructive testing enables scientists and engineers to evaluate the integrity of their structures and the properties of their materials or components non-intrusively, and in some instances in real-time fashion. Applying the Nondestructive techniques and modalities offers valuable savings and guarantees the quality of engineered systems and products. This technology can be employed through different modalities that include contact methods such as ultrasonic, eddy current, magnetic particles, and liquid penetrant, in addition to contact-less methods such as in thermography, radiography, and shearography. This book seeks to introduce some of the Nondestructive testing methods from its theoretical fundamentals to its specific applications. Additionally, the text contains several novel implementations of such techniques in different fields, including the assessment of civil structures (concrete) to its application in medicine.

InTech Europe
University Campus STeP Ri
Slavka Krautzeka 83/A
51000 Rijeka, Croatia
Phone: +385 (51) 770 447
Fax: +385 (51) 686 166
www.intechopen.com

InTech China
Unit 405, Office Block, Hotel Equatorial Shanghai
No.65, Yan An Road (West), Shanghai, 200040, China
中国上海市延安西路65号上海国际贵都大饭店办公楼405单元
Phone: +86-21-62489820
Fax: +86-21-62489821

IntechOpen